AALBORG UNIVERSITET
STUDENTERRAPPORT

Overexpression and secretion of PET-hydrolysing enzymes in *Pseudomonas putida* KT2440

Master Thesis

Enrico Porotti
MSc Engineering (Sustainable Biotechnology)

Supervisors: Cristiano Varrone & Virender Kumar

Submitted on: 20 December 2023

Abstract

Enzymatic plastic hydrolysis has recently surfaced as a promising new approach for plastic recycling. As with other proteins, the cost of industrial production of plastic-depolymerising enzymes is strongly affected by the final protein concentration, purification of the protein of interest from the rest of the biomass, and substrate price. *Pseudomonas putida* KT2440 is a soil-borne bacterium suited for industrial biotechnology and capable of fast growth on poor substrates. In this project, a plasmid carrying a fusion of the improved PET-hydrolysing enzyme $LCC^{ICCG-KRP}$ with a N-terminal signal peptide for periplasm localisation was assembled and used to transform *P. putida*. No strong evidence for secretion of the enzyme could be collected, but $LCC^{ICCG-KRP}$ was successfully purified from *P. putida*. PET depolymerisation assays revealed that the enzyme expressed by *P. putida* KT2440 has an activity comparable to that of $LCC^{ICCG-KRP}$ expressed in *E. coli*, with weight losses from amorphous PET of around 20% in a 72 h-long reaction at 70 °C with less than 2% the amount of enzyme required for the standardised depolymerisation assay. Approaches for the improvement of expression and engineering of secretion of heterologous proteins in *P. putida* KT2440 are also discussed.

Table of Contents

Abstract 2

Introduction 4

The case for enzymatic plastic recycling 4

Secretion of proteins in Gram negative bacteria 6

Materials and methods 8

Bacterial strains, media and growth conditions 8

Other chemicals and reagents 9

Instruments 10

Growth conditions 10

DNA manipulation 10

Plasmids 11

Assembly of expression vectors 11

Transformation of *E. coli* 13

Transformation of *P. putida* 13

Protein expression 13

Purification of LCC 15

Diafiltration of LCC 15

SDS-PAGE 16

Colorimetric protein quantification 16

Enzymatic activity assays 16

Results and discussion 16

Assembly of expression vectors 16

Protein expression studies 20

First expression study 20

Second expression study 22

Third expression study 24

Fourth expression study 26

Purification of $LCC^{ICCG\text{-}KRP}$ 27

PET depolymerisation assays 30

Future perspectives 34

Conclusions 36

References 36

Appendix 44

A. Protein-coding sequences submitted, codon-optimised for *P. putida* 44

B. Maps of plasmids received by Gene Universal and assembled expression vectors 45

Introduction

Since their introduction to the masses in the 1950s, plastic polymers have become widespread materials, with total plastic production in the 1950 – 2021 period estimated at almost 10 billion tons [PlasticsEurope, 2022]. The most produced polymers are polyethylene (PE), polypropylene (PP), polyvinylchloride (PVC), and polyethylene terephthalate (PET). The major use case for plastics is packaging (mostly PE, PP, and PET) followed by construction (mostly PVC), with PET also being heavily represented as a component of plastic fibres [Geyer et al, 2017]. Projections of current trends put annual plastic production at 1.1 billion tonnes in 2050 [Geyer, 2020]. Only about 9% of plastics ever produced is estimated to have been recycled, with most of the rest estimated to have become waste [Geyer et al, 2017] while the percentage of plastic entering a closed loop is even lower [McGlade et al, 2021]. The main reasons for low recycling rates include the lack of collection of plastic waste, and the high cost of recycling operations, largely caused by the high diversity of plastic polymers present in the market, often combined in the same product [World Bank Group, 2022]. In the case of thermoset plastics (e.g., polyester resins and PU), the loss of the chemical structure of the material upon exposure to high temperatures, makes recycling with current processes difficult [McGlade et al, 2021]. The presence of additives, including banned persistent organic pollutants, may hinder the process or reduce the quality of the recycled material [Leslie et al, 2016].

Plastic recycling is mainly done by mechanical recycling and chemical recycling. In mechanical recycling, the plastic waste is pelleted and re-extruded to a material with similar characteristics. Whereas in chemical recycling, polymers are broken down in thermal (i.e., pyrolysis or gasification) or chemolysis (e.g., hydrolysis or glycolysis) processes yielding shorter-chain compounds that can be used as fuel or as feedstocks for chemical syntheses [Ragaert et al, 2017; Okan et al, 2019].

Mechanical recycling is the most common route for recycling plastics but is generally limited to PET and PE plastics. Other polymers (such as PP and PVC) do not have the needed physical properties when melted or, as is the case for thermosets, their chemical structure is incompatible with re-melting. Polymers are often immiscible and even small amounts of contaminants in a specific plastic type result in a phase-separated mixture of lower quality than the virgin pure plastic, even to the point of the recycled material being unusable [Garcia & Robertson, 2017]. Because of this, plastic streams of high purity and clear of organic contaminants are prerequisites for mechanical recycling to succeed, limiting the applicability of this approach when dealing with post-consumer plastic waste [Ragaert et al, 2017]. The high temperatures and intense physical processing in mechanical recycling result in the shortening of polymer chains which degrades the quality of polymers at every cycle [Al-Salem et al, 2009].

Chemical recycling is generally hampered by high operating costs due to energy use or, in the case of low-temperature pyrolysis, due to the cost of chemical catalysts. Additionally, the products of some chemical recycling processes, especially pyrolysis, are not pure compounds but rather complex mixtures of compounds of different molecular weight [Zhang et al, 2021]. With particular reference to chemical recycling, which has the highest potential for material recovery and is therefore most interesting from a sustainability point of view, research is being conducted on the design and development of processes with lower energy requirements, and catalysts with higher specificity to obviate the need for high purity inputs [Garcia & Robertson, 2017; Huang et al, 2022]. Complex mixtures of different polymers are problematic for chemical recycling as well due to difficulties in purifying monomers and other break-down products [Zhang et al, 2021].

The case for enzymatic plastic recycling

Enzymes are highly specific catalysts that could in principle replace inorganic catalysis in depolymerizing plastic waste. Enzymatic depolymerization can be performed at far milder conditions compared to solvolysis, thus enzymatic depolymerisation can potentially overcome both the main challenges hampering plastic chemical recycling. Several organisms have been reported to have the ability to feed on plastics suggesting the existence of enzymes capable of degrading plastic polymers [Zhang et al, 2021]. Larvae of insects in the genus Tenebrio have been shown to eat PS and PE, with various gut bacteria (e.g., *Enterobacteriaceae*, *Citrobacter sp.*, *Kosakonia sp.*) reported as associated with degradation of the ingested plastic and evidence that the phenomenon is not limited to specific locales [Yang et al, 2015a; Yang et al, 2015b; Brandon et al, 2018; Yang et al, 2018].

The apparent ability of the larvae of another insect, the wax moth *Galleria mellonella*, to degrade PE was recently shown to be linked to two salivary enzymes of the phenol oxidase family catalysing the oxidation and chain-shortening of PE without pretreatment and at neutral pH and room temperature [Sanluis-Verdes et al, 2022]. The exact mechanism of action of the enzymes was not delved into, but the authors made the

argument that the enzymes, which appear to be involved in the detoxification of plant phenolics often present in pollen, catalyse the degradation of aromatic additives used to stabilise PE chains, with the concomitant release of free radicals leading to the observed chain-shortening. The exact role of the larval gut microbiome in PE degradation, and even whether the assimilation of PE occurs in *G. mellonella* are still debated, underlining the difficulties of clearly establishing mechanistic models for plastic polymers degradation [Réjasse et al, 2022].

It should be noted here that enzymes are never 100% specific. While a primary reaction can be identified and is catalysed at a high rate, it is still possible to observe secondary reactions, similar in their mechanisms to the primary reaction, which are catalysed at a slower rate. This opens up the possibility of novel pathways evolving from already existing ones and for the engineering of enzymes to improve side activities [Hedstrom, 2010].

Various plastic-degrading enzymes of microbial origin have been identified over the years and an updated list of characterised plastic-degrading enzymes can be found I the PAZy database (https://pazy.eu) [Bucholza et al, 2022]. The enzymes entered on PAZy so far have been reported to degrade bio-based polymers, PET, and polyurethane. The database also includes enzymes reported as having oxidative action against PE, and a few enzymes able to degrade oligomers of polyamide are also reported. Degradation of PS, PVC, and PP has so far remained elusive (for a critical appraisal of the literature on these polymers, the reader can refer to [Chow et al, 2022]). With regard to PET, polymer degradation has been reported for a number of microbial enzymes in the α/β-hydrolase superfamily, with members of the esterase [Perez-Garica et al, 2023], lipase [Eberl et al, 2009], and cutinase [Herrero Acero et al, 2011] families having been characterized for PET depolymerization.

A breakthrough in the search for plastic-degrading enzymes occurred in 2016 with the discovery and isolation, in a plastic bottle-recycling facility, of the first bacterium, subsequently named *Ideonella sakaiensis* 201-F6, shown to assimilate PET and use it as sole carbon source [Yoshida et al, 2016]. The catabolic pathway for PET depolymerization and assimilation was found to rely on two enzymes termed PETase (subsequently IsPETase) and MHETase. IsPETase was shown to catalyse the breakdown of PET polymers to mono-(2-hydroxyethyl)-terephthalic acid (MHET) and small amounts of terephthalic acid bis-(2-hydroxyethyl)-terephthalic acid (BHET), while MHETase hydrolyses MHET to terephthalic acid and ethylene glycol.

Further work was strengthened by the availability of metagenomic tools to actively mine for plastic-depolymerizing enzymes from environmental samples, thus tapping into the vast diversity belonging to non-culturable microbes. One notable example of this is the discovery of a PET-degrading enzyme that has been termed leaf-branch compost cutinase (LCC) as it was part of a metagenome sequenced from a compost heap [Sulaiman et al, 2012]. LCC has since been reported as having improved thermostability and PET-depolymerisation activity compared to other PET-degrading cutinases [Tournier et al, 2020]. In line with other cutinases, and contrary to IsPETase, LCC depolymerizes PET to terephthalic acid and ethylene glycol [Brandenberg et al, 2022].

So far, the identified PET-degrading cutinases share a disulfide bridge towards their C-terminus, with an intramolecular metal binding site for further stabilisation of the protein and leading to their classification as thermophilic proteins [Lu et al, 2020]. On the other hand, IsPETase was shown to have two disulfide bridges, one corresponding to the C-terminal bridge found in thermophilic cutinases and an intramolecular one replacing the metal binding site [Brott et al, 2022]. The additional disulfide bridge is thought to stabilize the active site which is characterized by a neighbouring “wobbly” tryptophan instead of the histidine observed in thermophilic cutinase. This substitution in turn is thought to determine a higher flexibility of the substrate binding site of IsPETase allowing it to adapt its conformation to the rigid structure of less amorphous PET [Fecker et al, 2018].

Since their discoveries, both LCC and IsPETase have been the subject of intense protein engineering efforts to improve their performances. Because the degree of crystallinity of PET is reduced at temperatures at or above its glass transition temperature (~70 °C), efforts have been focused on increasing the thermostability of the enzymes [Lu et al, 2022], although this seems to have also resulted in improved activity in most cases. For LCC, a highly thermostable variant was developed by a targeted engineering approach, incorporating two substitutions of surface-exposed amino acids, and engineering an internal disulfide bridge imitating the one described for IsPETase [Tournier et al, 2020]. Engineering the disulfide bridge, in place of the native metal binding site, eliminated the need to stabilise the enzyme by addition of divalent cations to the reaction mixture.. The resulting enzyme, called LCC^{ICCG}, was further refined by rational design

based on the crystal structure of the enzyme and the substrate-binding mechanism [Zeng et al, 2022]. This resulted in the $LCC^{ICCG-KRP}$ variant with even higher thermostability attributed to the substitution of a further surface-exposed amino acid and the establishment of two additional hydrogen bonding interactions inside the protein. However, there are no reports of engineering LCC at the wobbly tryptophan residue as seen in IsPETase.

Engineering of IsPETase employed targeted mutations based on structural insights of this and similar proteins and its substrate-binding mode to improve activity and thermal stability [Joo et al, 2018; Son et al, 2019; Zhong-Johnson et al, 2021], algorithmic design (which notably resulted in the DuraPETase [Cui et al, 2021] and FAST-PETase [Lu et al, 2022] variants), and directed evolution based on construction of mutant libraries by PCR (which resulted in the DepoPETASE [Shi et al, 2023] and HotPETase [Bell et al, 2021] variants; see also, [Brott et al, 2021]).

Some simulation studies and life-cycle assessments of enzyme-based chemical recycling of PET waste have been conducted to assess the economic feasibility and environmental impact of enzymatic PET recycling. An early suggestion for a process employing enzymatic hydrolysis of PET was modelled as using extruded and ground PET flakes as a substrate for batch depolymerization using LCC^{ICCG} with the recovery of terephthalic acid as the main product, and ethylene glycol and sodium sulphate as co-products [Singh et al, 2021]. In a later publication, the same process was used as the starting point for a plastic biorefinery concept with PET and cellulose as feedstocks, and bio-based polytrimethylene terephthalate and polyethylene furanoate as products [Roux & Varrone, 2021]. None of these processes was estimated to be economically competitive versus fossil-based PET production, with utilities and feedstock (especially sorted and clean PET) being the primary drivers of costs.

It is noticeable that in both papers the cost of the enzyme was reported as not being a significant factor in determining operating costs, with assumed prices of LCC^{ICCG} of 15 USD/kg [Singh et al, 2021] and 25 USD/kg [Roux & Varrone, 2021]. In both cases, it seems that the cost was assumed from techno-economical assessments of enzyme production by filamentous fungi. Techno-economical assessments for industrial enzyme production using bacterial hosts are not easy to find in the literature, but a baseline scenario of 316 USD/kg for β-glucosidase production from *E. coli* in Brazil, with glucose and ammonia as C and N source, respectively, has been reported [Ferreira et al, 2018]. A major driver of costs was found to be the need for lysing cells and purifying the enzyme from cell debris. Assuming that the enzyme could be secreted led to a reduction in production costs from 316 USD/kg to 289 USD/kg. Further reductions in production costs, to slightly more than the costs for fungi-based production systems, could be obtained by using a cheaper C source and by improving enzyme titres to avoid having to up-concentrate the purified enzyme. This underlines the importance of selecting and developing appropriate recombinant hosts, being able to utilise cheap substrates, producing high yields of proteins, and achieving secretion of the enzymes.

Pseudomonas putida KT2440 is a Gram-negative soil bacterium, a derivative of the *P. putida* mt-2 strain by way of losing the pWW0 toluene-degrading plasmid [Martins dos Santos et al (2004); Burlage et al (1989)]. *P. putida* is characterized by flexibility in the use of substrates, being able to use a vast array of compounds characteristic of organic waste materials as carbon sources, high resistance to oxidative stress, and lack of pathogenicity towards both animals and plants. An obligate aerobe, the carbon metabolism of *P. putida* is centred around the Entner-Doudoroff pathway which, along with the pentose phosphate pathway, shows high rates of NAD(P)H regeneration, in turn explaining the high resistance to oxidative stress [Martínez-Garcia et al (2014)]. Of relevance for industrial applications, *P. putida* KT2440 is well adapted to transient (2.6 s) glucose starvation, which is probably linked to the ability of the bacterium to accumulate polyhydroxyalkanoates and to quickly mobilise this carbon reserve when other carbon sources become depleted [Ankenbauer et al, 2020].

P. putida is also receptive to genetic modifications and numerous tools for synthetic biology have been developed for it, ranging from plasmid vectors with varying origins of replication [Cook et al, 2018], to transposons and integrative plasmids for insertion of DNA sequences in the chromosome [Volke et al, 2020; Martínez-García et al, 2011], to genome editing tools based on I-SceI and CRISPR/Cas9 [Wirth et al, 2020; Aparicio et al, 2018].

Secretion of proteins in Gram negative bacteria

In Gram negative bacteria, protein secretion is defined as the transport of proteins across the outer membrane; transport through the inner membrane to the periplasm can be part of the secretion process, but is otherwise not considered actual secretion [Filloux, 2022]. With this definition in mind, nine numbered secretion systems have been described in Gram-negative bacteria and bacteria with double-membrane cell

envelopes (that is the case for the type 7 secretion system found in Mycobacteria). Most of these, namely the T1SS, T3SS, T4SS, T6SS, T7SS, and T9SS, are involved in virulence and microbial competition, inserting effector proteins into target cells [Green & Mecsas, 2016]. In general, a secretion system consists of a proteinaceous channel extending through the cell's membranes and into the extracellular milieu (or target cell), ATPases to power protein secretion, and chaperones needed to maintain substrate proteins in a secretion-competent state.

Many secretion systems are evolutionarily linked to structures found on the outer cell surface. For instance, the T2SS shares many structural similarities with type IV pili [Douzi et al, 2012], and the T3SS can be understood to derive from the flagellar machine and its assembly mechanism, i.e., the flagellar type 3 secretion system or fT3SS [Abby & Rocha, 2012].

Secretion systems can be grouped in one-step and two-step pathways. The former group includes T1, T3, T6, T7, T8, and T9SS, which transport their substrates directly from the cytosol to the extracellular milieu or to target cells. T2SS and T5SS are two-steps pathways, as their substrates need to be translocated to the periplasm through either the general secretion pathway (Sec) or the twin arginine translocation pathway (Tat). Conflicting results on this topic have been found for the T4SS which generally acts as a one-step secretion pathway but, in *Bordetella pertussis*, is a two-step pathway, secreting toxins that are first transported to the periplasm [Filloux, 2022].

Recognition of substrate proteins by the Sec and Tat pathways is well understood and is based on the presence, at the N-terminus of a protein, of a short peptide called a signal peptide (SP). A typical SP for either pathway consists of three regions: a N-terminal n region which is positively charged, a middle hydrophobic h region, a C-terminal polar c region [Freudl, 2018; Erkut, 2021]. SPs for the Tat pathway tend to be longer and less hydrophobic, especially within the h region, compared to SPs that direct proteins to the Sec pathway; more notably, though, Tat pathway SPs have a specific motif, S/T-R-R-X-F-L-K, which is conspicuously absent in Sec pathway SPs and is found around the boundary between the n and the h region [Erkut, 2021]. Due to these similarities between SPs for Sec and Tat, tools for the prediction of signal peptides from amino acid sequences have been developed, most notably SignalP, now in its sixth version [Teufel et al, 2022].

In prokaryotes, once a protein has been exported to the periplasm, the signal peptide is usually cleaved by one of three signal peptidases, numbered I to III. The prevalent model for the cutting site of SPase I is the A-X-A rule, which lists the three C-terminal amino acids in the c region of signal peptides [Erkut, 2021]. However, it was shown by von Heijne and Abrahamsén (1989), that differences exist between species in terms of SPase I specificities [von Heijne & Abrahamsén, 1989], even leading to cases of aberrant processing of signal peptides when expressing heterologous proteins [Suominen et al, 1987]. More recently, it has been found that the SPs in certain taxa (e.g., Alphaproteobacteria) significantly deviate from the A-X-A rule, with amino acids other than alanine being the preferred residues in the SPs' c regions, something that has been linked to the low prevalence of alanine in those bacteria's genomes [Payne et al, 2012] and which calls for care when selecting signal peptides for heterologous protein localisation to the periplasm.

Secretion of heterologous proteins could be of interest not just for enzymes production companies, but also in the field of protein research and engineering. As mutant libraries used for screening of enzyme variants can be in the thousands, simplifying the isolation of the protein of interest by secretion could be a viable approach for faster and cheaper screening protocols.

Within the context of enzymatic PET hydrolysis, this thesis presents an attempt at the plasmid-based expression of PET-depolymerising enzymes in *P. putida* KT2440 with targeted secretion of the heterologous enzymes to the growth medium. While the initial plan called for a quantitative description of the process of expression and secretion of PET-depolymerising enzymes in the chosen host, technical difficulties led to a downsizing of the project's ambition. Expression of an LCC variant as reported in Brandenberg et al (2022) seems to have been replicated here, although no quantitative description of the process was possible in the end. Some observations about the literature on protein secretion in Gram negative bacteria are also presented, as the existence of secretion of heterologous periplasmic proteins was found to be dubious.

Materials and methods

Bacterial strains, media and growth conditions

The strain *E. coli* BL21 (DE3) was used for maintenance of all plasmids harbouring the synthetic gene constructs with our genes of interest (GOI). This is generally considered a sub-optimal choice owing to the strain expressing both endonuclease I and recombinase A in active form. Moreover, compared to *E. coli* BL21, the chromosome of the BL21 (DE3) strain has been modified by insertion of the T7 RNA polymerase gene, which leads to high basal expression of the coding regions (CDS) under control of the T7 phage promoter [Studier et al, 1990]. Availability of this strain and experience with it, due to its use as heterologous protein expression host in the group, were the reasons for its adoption despite its potential shortcomings. No apparent degradation or recombination involving the plasmids were observed.

P. putida KT2440 was ordered from Leibniz Institute DSMZ (DSM no. 6125, classified as *P. alloputida*) and kept as a cryostock at -80 °C until used.

Table 1 List of bacterial strains used in this project.

Strain	Genotype	Use	Source
***E. coli* BL21 (DE3)**	*F^- ompT gal dcm lon $hsdS_B(r_B^-m_B^-)$ λ(DE3 [lacI lacUV5-T7p07 ind1 sam7 nin5]) $[malB^+]_{K-12}(\lambda^S)$*	Maintenance of GOI-harbouring plasmids	Leibniz Institute DSMZ
E. coli* BL21 (DE3) pET28a(+)·*SPpstu-LCC$^{ICCG-KRP}$-6XHis	*pET28a(+)·SPpstu-LCC$^{ICCG-KRP}$-6XHis F^- ompT gal dcm lon $hsdS_B(r_B^-m_B^-)$ λ(DE3 [lacI lacUV5-T7p07 ind1 sam7 nin5]) $[malB^+]_{K-12}(\lambda^S)$*	Maintenance of pET28a(+)·*SPpstu-LCC$^{ICCG-KRP}$-6XHis* plasmid	This study
E. coli* BL21 (DE3) pET28a(+)·*SPpstu-IsP^{FAST}-6XHis	*pET28a(+)·SPpstu-IsP^{FAST}-6XHis F^- ampT gal dcm lon $hsdS_B(r_B^-m_B^-)$ λ(DE3 [lacI lacUV5-T7p07 ind1 sam7 nin5]) $[malB^+]_{K-12}(\lambda^S)$*	Maintenance of *pET28a(+)·SPpstu-IsP^{FAST}-6XHis* plasmid	This study
***E. coli* K-12 CC118 pSEVA238**	*pSEVA238 F^- LAM^- araD139 Δ(ara leu)7697 Δ(lacX74) phoA20(del) galE galK thi rpsE rpoB argE(Am) recA1*	Maintenance of pSEVA238 plasmid	SEVA Collection Team
***E. coli* K-12 CC118 pSEVA258**	*pSEVA258 F^- LAM^- araD139 Δ(ara leu)7697 Δ(lacX74) phoA20(del) galE galK thi rpsE rpoB argE(Am) recA1*	Maintenance of pSEVA258 plasmid	SEVA Collection Team
***P. putida* KT2440**	*rmo^- mod^+*	Wild type	DSMZ (nr. 6125)
***P. putida* 258·SP_{pstu}-LCC$^{ICCG-KRP}$-6XHis**	*pS258*·SP_{pstu}-LCC$^{ICCG-KRP}$-6XHis rmo^- mod^+*	P. putida KT2440-derivative harbouring the pS258·SP_{pstu}-LCC$^{ICCG-KRP}$-6XHis plasmid	This study

Sterile conditions when working with live cells and sterile media were maintained by use of a vertical laminar air flow bench equipped with a UV lamp, and 70% ethanol for disinfection. Unless otherwise stated, media, media components, glassware to be used with media or cultures, plastic pipette tips not supplied as sterile, and Eppendorf tubes were generally sterilised by autoclaving at 121 °C for at least 15 minutes. All

single-use items that come in contact with media or cultures (e.g., Falcon tubes, inoculation loops, L-spatulas, Petri dishes, syringes and syringe attachments, multi-well microplates, breathable membranes for microplates) were acquired as sterile from the suppliers.

The growth medium for most liquid bacterial cultures was lysogeny broth (LB) (Miller) medium: 10 g/L NaCl, 10 g/L soya peptone, 5 g/L yeast extract. Agar plates were prepared by addition of 2% agar to LB (Miller). Liquid LB and poured plates were stored at 4 °C when not in use.

A minimal salt medium (MSM) was also prepared with the composition reported in Table 2. The concentrated stock of trace elements was vacuum filtered through a 0.22 µm filter. A 200 mM glucose working stock, vacuum filtered, was used as sole carbon source, with a final concentration of 20 mM glucose in the growth medium. The glucose solution and the phosphate buffer were stored at 4 °C, while the trace elements solution was stored at room temperature with the bottle wrapped in foil. The concentrated stock solutions were mixed as needed and diluted to the correct final concentrations with autoclave-sterilised dH_2O.

A 50 g/L stock of kanamycin (Km), stored at -20 °C when not in use, was added to liquid media in a 1:1000 dilution. Selective agar plates were prepared by adding Km in the same dilution rate to molten agar that was left to cool to approximately 55 °C.

Table 2 Composition of MSM medium.

Solution	Component	Final concentration [mg/L]
Phosphate buffer (+N)	K_2HPO_4	3880
	NaH_2PO_4	1630
	$(NH4)_2SO_4$	2000
Trace elements	EDTA (disodium salt)	10
	$MgCl_2 \cdot 6H_2O$	100
	$ZnSO_4 \cdot 7H_2O$	2
	$CaCl_2 \cdot 2H_2O$	1
	$FeSO_4 \cdot 7H_2O$	5
	Na_2MoO_4	0.17
	$CuSO_4 \cdot 5H_2O$	0.2
	$CoCl_2 \cdot 6H_2O$	0.4
	$MnCl_2 \cdot 4H_2O$	1.22
Glucose 200 mM	Glucose	3600
Kanamycin 50 g/L	Kanamycin	50

Other chemicals and reagents

All reagents used were of analytical grade and supplied by Merck, VWR, Thermo Fisher Scientific, Fluka, GenScript, or Acros Organics. A TE buffer (elution buffer) was used during DNA purification and for resuspension of primers. It was prepared with 1.211 g/L of Tris and 0.292 g/L of EDTA (pH 8.0) with HCl. The solution was autoclaved and stored at 4 °C when not in use. PCR, restriction, and ligation reactions were prepared with PCR-grade water from Thermo Fisher Scientific or nuclease-free water from Omega Bio-Tek as diluent.

50X TAE buffer from PanReac AppliChem was diluted with dH_2O and used for the casting of gels with 4% agarose (Invitrogen) and as running buffer for gel electrophoresis of DNA. Before casting, the gels were stained with SYBR Safe dye from Thermo Fisher Scientific. Ladders used for gel electrophoresis were either GeneRuler 1kb or ZipRuler Express 1, both from Thermo Fisher Scientific. DNA samples other than DreamTaq PCR products were mixed with 5X GelPilot DNA loading dye (QIAGEN) or 6X purple loading dye (NEB) before being loaded in agarose gels.

A 4X modified Laemmli sample buffer for protein analysis was prepared, per 100 mL, with 40 mL glycerol, 20 mL 1M Tris (pH adjusted to 6.8), 8 g SDS, 400 mg bromophenol blue. When not in use, this was stored at -20 °C. Tris-MOPS-SDS running buffer from GenScript was reconstituted in dH_2O for SDS-PAGE electrophoresis.

Three potassium phosphate ()KPO) buffer solutions were used for protein purification by immobilized metal affinity chromatography (IMAC):

Table 3 Composition of buffers for protein purification by IMAC. All were adjusted to pH 7.5.

Solution	KPO [mM]	Imidazole [mM]	NaCl [mM]
Binding buffer	50	5	300
Wash buffer	50	20	300
Elution buffer	50	200	300

A chemical lysis buffer was prepared in-house, based on a paper by [Danilevich et al, 2006], with 50 mM Tris, 150 mM NaCl, 1% Triton X-100, 5 mM EDTA and pH adjusted to 8.0.

3-methylbenzoate (3-mBZ) was the compound chosen for induction of heterologous gene expression in *P. putida*, using a 0.5 M, pH 7.0, filter-sterilised working stock of the compound which was stored at room temperature until needed.

Instruments

Optical density measurements and colorimetric assays were generally performed with a VWR V-1200 spectrophotometer equipped for visible-light spectroscopy. A Bio-Rad SmartSpec Plus spectrophotometer was also used for OD_{600} measurements in connection with preparing electrocompetent *E. coli* cells. Ahead of starting the induction experiments, growth curves of *P. putida* 258·SP_{pstu}-$LCC^{ICCG\text{-}KRP}$-6XHis were obtained from incubation in a Bio Tek Epoch 2T microplate reader. A Bio-Rad S1000 thermocycler was used for all PCR and restriction reactions. A NanoDrop ND-1000 and a NanoDrop One by Thermo Fisher Scientific were used for quantification of DNA and proteins. All gels, whether loaded with DNA or proteins, were imaged with a Chemi Doc MP imager with Image Lab software for image acquisition and processing. Bacteria transformation was done by electroporation on an Eppendorf 2510 electroporator, voltage set at 2500 V, 10 µF capacitance, 600 Ω internal resistor. Electrocompetent cells and plasmids were mixed in 0.1 cm gap width cuvettes sterilised with 70% ethanol. IMAC was performed with a 5 mL HisTrap™ HP column (Cytiva) on an ÄKTA™ start chromatographer (GE Healthcare Bio-Sciences).

Growth conditions

For early detection of contaminations in *P. putida* cultures, cetrimide agar plates (a *Pseudomonas*-selective medium) were prepared from a ready-made mix (Merck). This was dissolved in deionised water on a magnetic stirrer heated to about 70 ℃ and reagent-grade glycerol (Acros Organics) added to a 1% final concentration prior to autoclaving. The poured plates were stored at 4 °C until needed. As a further mean of detecting contaminations, liquid growth media were at times incubated in 50 ml Falcon tubes without inoculum for at least 16h and visually inspected for microbial growth.

For long-term storage of bacteria, liquid cultures were supplemented with sterile glycerol to a final concentration of 20%, snap-frozen in liquid nitrogen and stored at -80 °. Liquid overnight cultures (16h incubation) and inoculated agar plates were stored at 4 °C and used as ready sources of inoculum.

Incubation conditions were 37 °C with orbital shaking at 190 rpm for *E. coli*, while *P. putida* was incubated at 30 °C with orbital shaking at 200 rpm in an IKA KS 4000 i control incubator.

DNA manipulation

Extraction of plasmid DNA from bacterial cells was done with either Omega Bio-tek E.Z.N.A. Plasmid Mini-kit I or Macherey-Nagel NucleoSpin Plasmid Mini-kit according to manufacturers' instructions. The elution of DNA was done with the provided elution buffers or the in-house TE buffer. All DNA solutions in water were

stored at -20 °C when not in use. Q5 DNA polymerase, restriction enzymes and T4 DNA ligase were acquired from NEB, while DreamTaq Green PCR master mix was acquired from Thermo Fisher Scientific. Restriction reactions were prepared with the rCutSmart or r3.1 buffers supplied with the enzymes, while ligation reactions were performed with the T4 DNA ligase buffer supplied with the enzyme. Clean-up of DNA after enzymatic reactions was carried out with Macherey-Nagel Gel and PCR Clean-up Mini-kit according to manufacturer's instructions, using the provided buffer for elution.

Plasmids

The choice of plasmid backbones for expression of PET hydrolases in *P. putida* KT2440 fell on two plasmids from the SEVA family, namely pSEVA238 and pSEVA258. SEVA (Standard European Vector Architecture) is repository maintaining and managing a family of standardised plasmids each characterized by a selection marker module, origin of replication module, cargo module, T1 and T0 terminators, origin of conjugation, and six universal primer-binding sequences flanking the modules [Silva-Rocha et al, 2013; Martínez-García et al, 2023]. Restriction sites, flanking the modules and within the MCS, are also standardised between the different vectors to facilitate cloning of new genes in the plasmids and swapping of modules.

Both plasmids contain a kanamycin resistance gene, while the cargo module is a XylS/*Pm* expression system. The XylS/*Pm* system has its origin from the pWW0 toluene degradation plasmid from *P. putida* mt-2, the parent strain of KT2440. The promoter *Pm* is an inducible promoter activated by the binding of the XylS protein to two sites, one with binding at positions -39 and -49 on the promoter, one with binding at positions -60 and -70. Activation of XylS requires a benzoate-derived inducer, the most commonly used being 3-methylbenzoate (3-mB; also known as m-toluate) [Gawin et al, 2017], which is well tolerated by *P. putida*.

The two plasmids differ in their origin of replication, with pSEVA238 harbouring the pBBR1 ori (medium copy-number in *P. putida*) and pSEVA258 having the RSF1010 ori (high copy-number in *P. putida*) [Cook et al, 2018]. This choice was motivated by the consideration that protein expression levels can be influenced by plasmid copy numbers, which in turn could affect the dynamics of protein translocation, secretion and aggregation.

The plasmids were ordered directly from SEVA and received in the form of agar stabs harbouring E. coli K-12 CC118 [Manoil & Beckwith, 1985] transformed with either of the plasmids.

Table 4 List of plasmids used in this work.

Plasmid	Features	Source
pET28a(+)·SP_{pstu}-$LCC^{ICCG-KRP}$-6XHis	ori(f1) oriV(pBR322) Km^R rop P*lac*→lacI T7lac→SP_{pstu}:$LCC^{ICCG-KRP}$:6XHis 6XHis	Gene Universal
***pET28a(+)*·SP_{pstu}-IsP^{FAST}-6XHis**	ori(f1) oriV(pBR322) Km^R rop P*lac*→lacI T7lac→SP_{pstu}:IsP^{FAST}:6XHis 6XHis	Gene Universal
pSEVA238	oriT oriV(pBBR1) XylS *Pm* Km^R	SEVA Collection Team
pSEVA258	oriT oriV(RSF1010) XylS *Pm* Km^R	SEVA Collection Team
***pS258*·SP_{pstu}-$LCC^{ICCG-KRP}$-6XHis**	oriT oriV(RSF1010) XylS *Pm*→SP_{pstu}:$LCC^{ICCG-KRP}$:6XHis 6XHis Km^R	This study, derivative of pSEVA258

Assembly of expression vectors

The choice of PET-hydrolysing enzymes fell on $LCC^{ICCG-KRP}$ and FAST-PETase as the most promising enzymes at the time the project started. The sequences coding the two enzymes were fused, at their N-termini, to the signal peptide (SP) of *Pseudomonas stutzeri* MO-19's maltotetraose-forming amylase [Fujita et al, 1989], which has already been used as an N-terminal SP with PET-depolymerising enzymes [Lu et al, 2022]. The

sequences were codon-optimised on Benchling for expression in *P. putida* and a 6XHis-tag-coding sequence (six repetitions of the codon CAC), with a stop codon at its 3'-end, was added at the C-termini for purification of the proteins by immobilised metal affinity chromatography (IMAC). The sequences were then submitted to Gene Universal for synthesis and cloning into pET28a(+) vectors.

Restriction and ligation cloning was chosen for the assembly of expression vectors from the chosen empty SEVA plasmids. A first approach called for amplification of the sequences submitted to Gene Universal by PCR with primers pstu_F and Histag_R, The primers were designed with a HindIII and SpeI restriction site, respectively, in their 5'-overhangs. The amplified GOIs and the plasmids were to be digested with HindIII and SpeI-HF, followed by ligation with T4 DNA ligase. Once the expression and secretion plasmids had been assembled, secretion-negative plasmids were to be assembled by amplification of the GOIs using the primers FAST_F (for FAST-PETase) or ICCG_F (for $LCC^{ICCG-KRP}$) with Histag_R. The additional forward primers would have bound the GOIs downstream of the SP sequence, with 5'-overhangs containing an ATG codon preceded by a HindIII site. Restriction and ligation of the new coding sequences into the empty backbones would have followed the same procedure described above.

Table 5 List of primers used in this work. Overhangs are indicated by underlined nucleotides, with restriction sites absent in the target sequences indicated in bold.

Primer	Sequence
PS1	AGGGCGGCGGATTTGTCC
PS2	GCGGCAACCGAGCGTTC
pstu_F	**AAGCTT**GAATGAGCCACATCCTGCGAG
Histag_R	**ACTAGT**TTAGTGGTGGTGGTGGTGG
FAST_F	**AAGCTT**ATGCAGACCAACCCATACGCG
ICCG-F	**AAGCTT**GGATGAGCAACCCGTACCAGCGT
T7-pET-mod	CCCGCGAAATTAATACGACTCAC
pET24a	GGGTTATGCTAGTTATTGCTCAG
T7terminator-PstI	AA**CTGCAG**GCTAGTTATTGCTCAGCGG
T7term-SphI	A**GCATGC**CTAGTTATTGCTCAGCGGT

The first approach was found to not work as expected requiring the design of new primers. This was complicated by some limitations, presented in the "Results and discussion section", of the vectors received by Gene Universal. Standard primers were then considered as a work-around, with the final choice falling on T7-pET-mod and pET24a, which bind to the T7 promoter and T7 terminator sequences respectively. Following PCR with these primers (using a touch-down protocol for increased specificity [Korbie & Mattick, 2008]), digestion of the amplicons was done with the XbaI and XhoI enzymes. The backbone plasmids were double-digested with XbaI and SalI, and ligation of inserts and backbones was done with T4 DNA ligase making use of SalI and XhoI generating compatible sticky ends. This also allowed the cloning of the ribosome binding site (RBS) from the pET28a(+) backbone to the SEVA plasmids, since the pSEVAxx8 series lacks its own RBS on either side of the multiple cloning site (MC), a fact that was initially overlooked.

This approach also failed to yield results when *P. putida* was transformed with the ligation products. It was then decided to employ a new set of restriction enzymes for digestion of vectors and inserts and new reverse primers, T7terminator-PstI and T7term-SphI, were designed for amplification of the $LCC^{ICCG-KRP}$ and $IsPETase^{FAST}$ sequences, respectively; T7-pET-mod was still to be used as the forward primer in both pairs. In order to maximise the efficiency of the digestion reaction, extra nucleotides were added in the overhangs of these new primers to ensure sufficient distance between the end of the linear PCR product and the added restriction site. Due to the limited time remaining at this point, it was decided to focus on expression of $LCC^{ICCG-KRP}$ in pSEVA258. After amplification of the GOI by Q5 PCR, the amplicon and the empty vector were both digested with XbaI and PstI-HF, followed by ligation with T4 DNA ligase, to yield plasmid pS258·SP_{pstu}-$LCC^{ICCG-KRP}$-6XHis.

After transformation of *E. coli* BL21 (DE3) and *P. putida* KT2440 with this plasmid, colonies of putative successful clones were re-streaked on LB+Km agar plates and briefly incubated until growth was observable. Then a 1 µL loopful of biomass was suspended in 20 µL of a DreamTaq PCR mix with primers PS1 and PS2 and the resulting PCR product was loaded on agarose gel for electrophoresis and imaging.

The plasmid itself was later purified from an overnight liquid culture of the confirmed *P. putida* transformants using the mini-prep kit's elution buffer, and delivered to Eurofins Genomics for Sanger sequencing, with the PS1 and PS2 universal SEVA primers, to confirm the successful ligation of the GOI in the backbone.

Transformation of *E. coli*

Electrocompetent cells of *E. coli* BL21 (DE3) were prepared by growing to OD_{600} of 0.4 - 0.8 and repeated washing of the cells with sterile dH_2O followed by a single washing step with sterile 10% glycerol. The cells were kept at 4 °C during centrifugation and medium exchange. When not used straight away for transformation, the resulting suspension was kept at -80 °C. The transformation was then performed with 60 µL of the concentrated electrocompetent cells suspension and 0.5 µL of a plasmid DNA solution in electroporation cuvettes. The electroporated suspension was quickly supplemented with 1 mL of fresh LB medium and incubated for 1.5 h for recovery. Afterward, the suspension was spread plated on LB-Km agar plate which was incubated overnight.

Transformation of *P. putida*

Preparation of electrocompetent *P. putida* KT2440 cells was performed according to five protocols based on [Choi et al, 2006] and [Köbbing, 2020], eventually settling on the method of [Choi et al, 2006]. The variety of protocols used was due to repeated failures to obtain viable transformants which was eventually traced to a biological contamination of the working stock of *P. putida*.

The final protocol consisted of washing three times, with 300 mM sucrose, a 10 mL overnight culture of *P. putida* grown in LB, before resuspending the pelleted cells in 100 µL of 300 mM sucrose. The suspension was then either stored at -80 °C or kept on ice for transformations to be done on the same day.

For electroporation, the entire concentrated electrocompetent cells suspension is transferred to an electroporation cuvette along with 1 µL of a plasmid DNA solution. After electroporation, the suspension is quickly supplemented with 1 mL of fresh LB medium and incubated in round-bottom 13 mL tubes for 2 h to allow the cells to recover. Afterwards, the suspension is used to inoculate a LB-Km agar plate.

Protein expression

Expression in small scale

The growth curves of *P. putida* 258·SP_{pstu}-$LCC^{ICCG\text{-}KRP}$-6XHis were determined on a microplate reader to obtain optimum protein expression. The reader was programmed to maintain 30 °C, with continuous 3 mm orbital shaking at 425 rpm, 16 h runtime with 30 minutes intervals resulting in 33 measurements of OD_{600} in the wells.

A 12-wells Greiner CELLSTAR® plate covered with a Breathe-Easy® sealing membrane (Merck) was used as the culture vessel. Media used were LB and MSM with 20 mM glucose, both supplemented with Km. To avoid the possibility of oxygen becoming the limiting factor for growth in the plate, the working volume was chosen as 1 mL, which is less than the 2 - 4 mL nominal working volume for the plate used. Six wells were filled with the specified volume of each growth medium, with 5 out of 6 wells inoculated with a 1 mL inoculation loop of a concentrated suspension of cells harvested from an agar plate. The sixth well of each growth medium was used for blank correction.

All expression studies were started by inoculating the chosen growth medium with the required volume of an overnight culture, grown in LB with Km, to attain a starting OD_{600} of 0.1.

The first expression study was performed with MSM supplemented with Km and 20 mM glucose in 250 mL baffled flasks filled with 50 mL of inoculated growth medium. Four replicates of the culture were prepared, and the flasks incubated at the same time.

After approximately 1.5 h of incubation, the OD was again measured and found to exceed 0.4 in all but one replicate culture and 3-mBZ was added, at a final concentration of 0.5 mM, to start the induction. Samples were taken at 0 (i.e., right after addition of 3-mBZ), 2, 4, 9, and 24 h post-induction. OD_{600} was measured on all samples, followed by centrifugation to separate the cells from the supernatants. At the 24 h mark, what was left of the four cultures inside the flasks was collected in 50 mL Falcon tubes and pelleted by centrifugation. Pellets, supernatants, and the Falcon tubes were stored at 4 °C.

Expression in shake flasks

A second expression experiment was done with the same general procedure as the first study, with two 250 mL baffled flasks inoculated with the wild type *P. putida* KT2440 and two flasks inoculated with the plasmid-harbouring strain of *P. putida*. The growth medium for the transformant strain was supplemented with kanamycin, while this was omitted from the cultures of the wild type strain. All cultures were supplemented with 3-mBZ at a final concentration of 0.5 mM on reaching OD_{600} 0.4, but due to different growth rates between the two strains, the wild type cells were induced about 30 minutes before the transformants. The sampling scheme and treatment of samples were the same as for the first study, except that samples were taken 8, instead of 9, hours post-induction. Also, the cultures of the wild type strain were sampled at a 30 minutes delay to the nominal post-induction time so that cultures of the two strains could be sampled together.

Due to difficulties in observing clear patterns in SDS-PAGE gels that would indicate LCC expression, I decided to explore the possibility that tweaking the composition of the growth medium could result in higher levels of expression. Therefore, the third expression study was set up as an exploratory 2^{3-1} (resolution III) fractional factorial design with the concentrations of glucose, $(NH_4)_2SO_4$, and 3-mBZ as 2-level factors and four replicate centre points. The R package FrF2 (version 2.3-2) [Grömping, 2014] was used to generate the design as specified. For easier sampling and reduced disturbance of the cultures, two sets of 50 mL Falcon tubes were prepared, following the same experimental design, with one set withdrawn from the incubators 4 hours after induction, and the other set 8 h after induction. Based on results from the previous studies, induction was started 2.5 h after inoculation for all tubes without first measuring the OD.

Table 6 Meaning of factor levels and tested combinations of levels for the 2^{3-1} FFD for the effect of growth medium components on $LCC^{ICCG-KRP}$ expression.

Level	**Glucose [mM]**	**$(NH_4)_2SO_4$ [g/L]**	**3-mBZ [mM]**
-1	20	2	0.50
0	40	3	0.75
1	60	4	1.00
	Experimental scheme		
Experiment nr.	**Glucose**	**(NH4)2SO4**	**3-mBZ**
1	0	0	0
2	0	0	0
3	1	-1	-1
4	1	1	1
5	0	0	0
6	-1	-1	1
7	-1	1	-1
8	0	0	0

A fourth, and final, expression study was performed with LB medium to try increasing protein synthesis by using a richer growth medium. Eight 500 mL flasks (100 mL fill volume) were prepared, four inoculated with an over-night culture of P. putida KT2440, four with an over-night culture of *P. putida* 258·SP_{pstu}-$LCC^{ICCG-KRP}$-6XHis. For each strain, one flask was withdrawn from the incubator 1.5 h after inoculation (as 0 h post-induction) and at 2, 4, and 8 h post-induction. Expression was induced with 3-mBZ in a final concentration of 0.5 mM. Samples were withdrawn for OD_{600} measurement, and the cultures were then centrifuged to separate the cells from the growth medium.

Purification of LCC

Cell lysis by sonication
The cells were suspended in a lysis buffer and lysed by ultrasonication, on ice, with three 15 minutes cycles (9 s on, 10 s off, 50 % amplitude). The lysate was centrifuged (12000 g for 25 min) to remove cell debris.

Chemical lysis
A chemical lysis procedure was chosen instead of ultrasonication for quicker processing of the pelleted cells. The cells were resuspended in 2 mL of chemical lysis buffer and incubated at room temperature for 20 minutes. The suspension was then centrifuged to separate cell debris.

IMAC
IMAC was done manually on AKTA prime instrument and using 5 mL HisTrap FF column. The column was pre-equilibrated with lysis buffer. The sample was loaded at 1 mL/min flow rate, and a sampl of the flow-through was collected. The column was the washed with the wash buffer until the UV absorbance measured by the instrument's in-line UV sensor reached the baseline; a sample of the wash solution was collected from the waste outlet. A multi-step elution was performed by stepwise increasing the gradient with increasing proportions of the elution buffer and the eluate was fractionated to approximately equal volumes into three tubes

A protocol (Table 7) was then created on the instrument to automate the process, following guidelines from the column's manufacturer. Details of the method can be seen in *Table 7.* Contrary to the first protocol for IMAC, here a single-step elution was chosen, since only one protein was to be purified.

Table 7 Set-up of IMAC protocol for $LCC^{ICCG-KRP}$ purification on Äkta start chromatographer.

Setting		Value
Column volume		5 mL
Flow rate		5 mL/min
Sample volume		20 mL
Fractionation		6.2 mL
	Steps in IMAC protocol	
Equilibration	Binding buffer	5 column volumes (CV)
Sample loading		
Wash	Wash buffer	3 CV
Elution	Elution buffer	5 CV

Diafiltration of LCC

Buffer exchange and concentration of LCC purified via IMAC was done with Amicon® Ultra-15 centrifugal filter units. The filters are equilibrated with 50 mM potassium phosphate buffer (pH 8.0), then the eluate from the IMAC column is loaded on the filter and the tube centrifuged to let the eluate's buffer through the membrane. Three washing steps were then performed with the same potassium phosphate buffer used for the initial equilibration, 5 mL of buffer per step.

As the centrifuge used for this procedure was not refrigerated, the tubes were kept on ice for a few minutes between each centrifugation run. The retentate was then collected in an Eppendorf tube and stored at 4 °C until further use.

SDS-PAGE

Gel electrophoresis was the method of choice for detection of expressed protein in induced cultures of transformant *P. putida*. The cell suspension was prepared by mixing 10 µL of a cell suspension (OD_{600} 0.4), prepared by dilution of a culture sample, with 5 µL dH_2O and 5 µL of 4X sample buffer. Culture supernatant samples were prepared by addition of the 4X sample buffer to the untreated supernatant. All samples were incubated at 95 °C for 5 minutes.

SurePage™ gels (4 – 20% MOPS or 4 – 12% MOPS, depending on availability) from GenScript were loaded with either 20 µL of a cell suspension diluted to a final OD of 0.2, or with variable volumes of supernatants and fractions from IMAC of target proteins (actual volumes noted on pictures of gels). The Pierce™ unstained protein MW marker from Thermo Fisher Scientific was stored at -20 °C in small aliquots when not in use and employed as ladder for the gels in 5 µL volumes.

Electrophoresis was carried out until the indicator dye reached the bottom of the gel, about 1 h at 140 V. Staining of the gels was done with InstantBlue™ Coomassie stain from Kem-En-Tec Nordic with one hour incubation on a linear shaker. Destaining, while not strictly required with the chosen stain, was nonetheless performed with dH_2O, incubating the stain on a linear shaker for one hour or overnight.

Colorimetric protein quantification

Quantification of proteins in supernatants, IMAC eluates, and diafiltration retentates was generally done with the Pierce™ Bradford Plus protein assay kit from Thermo Fisher Scientific by following the manufacturers' instructions for either test tube (working range: 125 – 1000 µg/mL) or micro test tube (working range: 1 – 25 µg/mL) procedures. After incubation at room temperature, absorbance was measured at 595 nm and used to back-predict the concentration on proteins based on a calibration curve.

Enzymatic activity assays

Verification of enzyme activity was performed with p-nitrophenylbutyrate (p-NPB) as substrate for esterase enzymes in a 0.02 mM concentration in a 1 mL reaction mixture. 20 µL of a protein sample is added to the reaction mixture, and the presence of esterase activity is evaluated visually after 5 minutes at room temperature as the development of yellow colour due to the hydrolysis of p-NPB to p-nitrophenol.

PET depolymerization assay

PET depolymerisation with LCC was assessed on an amorphous PET film supplied by Goodfellow. The film is cut in, approximately, 0.5x1.0 cm pieces, aiming for a weight of 12 – 15 mg for each piece. The pieces are then washed with 0.5% Triton X-100, dH_2O, 0.1 M Na_2CO_3, and twice more with dH_2O. The film pieces are then lyophilised and weighed into pre-weighed 2 mL Eppendorf tubes. 1 mL of a mixture consisting of 0.05 mM KPO buffer (pH 8.0) and LCC diluted to a final concentration of 5 µM is added to the tubes, with 1 mL of 0.5 mM KPO buffer (pH 8.0) used as control. Finally, the tubes are incubated on a thermoshaker set at 70 °C and 700 rpm for a maximum of three days, after which the reaction buffer is discarded, the films and tubes are rinsed with dH_2O, and oven dried, in their tubes, at 60 °C to constant weight. The tubes are again weighed, and the percent weight loss of the films calculated.

Results and discussion

Assembly of expression vectors

As mentioned, the process for assembly of plasmid vectors went through various iterations. Fig. 1 shows the agarose gel from an early PCR, where lanes 1 to 4 present products of PCRs using the acquired plasmids as

templates, while wells 5 to 10 were loaded with products of colony PCRs from *E. coli* BL21 (DE3) transformed with the received pET28a(+)-based vectors. Besides the presence of non-specific products for most of the plasmids, probably caused by using the same annealing temperature (56 °C) for all reactions, none of the pET28a(+) plasmids had the correct product (expected to be around 900 bp in size).

It was then realized that Gene Universal had done its codon optimization of the submitted sequences, introducing mismatches in the chosen primer-binding sites. Furthermore, pET28a(+) contains two 6XHis-tags, one with sequence $(CAT)_6$ and one with sequence $(CAC)_6$, the latter being identical to the 6XHis-tag in the sequences submitted to Gene Universal. The direction in which the GOIs were cloned into pET28a(+) by Gene Universal meant that the 6XHis-tag of the GOIs was next to the almost identical 6XHis-tag from pET28s(+), creating multiple secondary binding sites for the initial reverse primer. Additional unforeseen secondary binding sites for the initial primer pair, some appearing within the GOIs themselves due to codon optimization, were found later on, with estimated Ta's close to the Ta's of primary binding sites.

Out of the six colony PCR products, five apparently did not leave their wells, which is usually attributed to an excess of cell debris left in the PCR mix, although the absence of amplification products in lane 7 confirms the issues with primers binding that were later identified. Products of colony PCR remaining in the wells were a recurrent problem with the protocol used to confirm transformation, however remained unidentified until the project was almost concluded. Centrifuging the PCR products before loading them in the gel should in general avoid this issue, but the glycerol in the DreamTaq master mix used for confirmatory colony PCRs would have also settled at the bottom, complicating the loading of samples in the gels.

A different protocol, in which cell suspensions are subjected to multiple freeze-boil steps, followed by centrifugation and using the supernatant as a template in PCR, was used to prepare DNA samples from bacterial colonies for Sanger sequencing. This protocol did not give any apparent problem when PCR products were loaded on gels. Alternatively, a PCR master mix without glycerol, requiring the post-PCR addition of a gel loading dye, could be used instead of DreamTaq Green PCR master mix to allow centrifuging the PCR products without loss of glycerol from the mix.

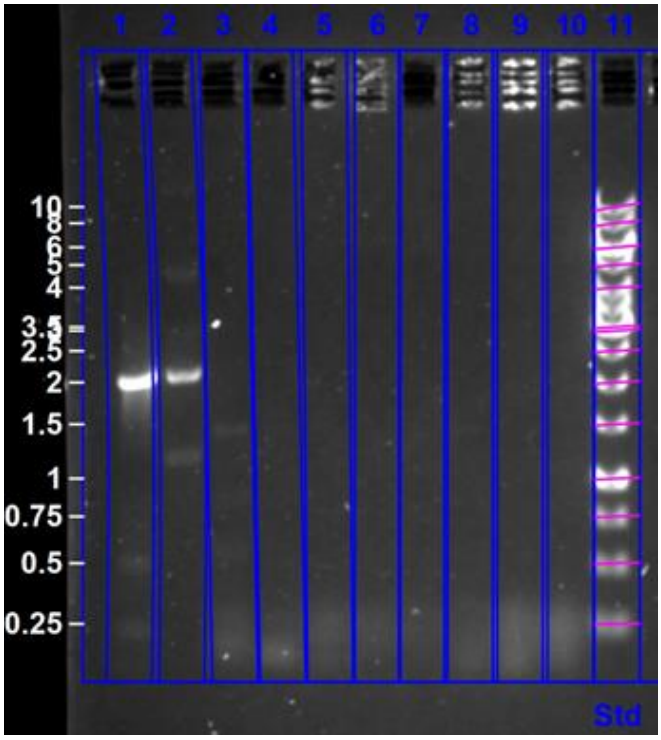

Fig. 1 Gel electrophoresis (4% agarose) of DreamTaq PCR products. Lanes 1 to 4 were loaded with amplicons of pSEVA238, pSEVA258 (both with primers PS1 and PS2), pET28a(+)·SPpstu-LCCICCGKRP-6XHis, pET28a(+)·SPpstu-IsPFAST-6XHis (both with primers pstu_F and Histag_R). Lanes 5 to 7 were loaded with amplicons from single colonies of E. coli BL21 (DE3) pET28a(+)·SPpstu-LCCICCGKRP-6XHis, lanes 8 to 10 with amplicons from single colonies of E. coli BL21 (DE3) pET28a(+)·SPpstu-IsPFAST-6XHis. The ladder, in lane 11, is GeneRuler 1 kb.

The second approach, digestion with XbaI plus XhoI on amplicons from pET28a(+)-based plasmids and digestion with XbaI and SalI on empty SEVA plasmids, yielded zero colonies on LB+Km plates after electroporation with the ligation products. It was concluded that the most likely cause was the combination of enzymes used for the double digests of insert and backbone. First, NEB cautions that sites cut by XhoI have low ligation efficiency. What is more, the non-improved isoschizomer of SalI, which was used in this approach, is not active in the rCutSmart buffer used for XbaI. As a work-around, the double digest of the plasmid backbone was run with the r3.1 buffer provided with SalI, which meant a lower efficiency for XbaI.

A further problem arose from the SalI and XbaI sites being next to each other on the chosen SEVA plasmids, with SalI reported as having no activity on cut sites located at the terminus of a DNA molecule. The combined losses of efficiency at both digestion and ligation likely resulted in very low amounts of correct assemblies. Early detection of issues at the restriction level was impossible to detect on agarose due to the small differences in size between undigested and digested DNA molecules.

Attempting to run the two restriction digestions sequentially, digesting first with SalI, followed by heat inactivation, then adding XbaI and running another digestion and inactivation program, likewise gave no result. A better alternative to this could have been to digest the backbone with SalI in r3.1 buffer, purify the linearised plasmid on silica columns, then run another digestion on the purified plasmid with XbaI in rCutSmart buffer. However, recovery of DNA from silica columns is never complete, and having additional rounds of purification would have resulted in additional losses of DNA, besides making the procedure more cumbersome.

This led to the third cloning approach, which also ran into some initial hurdles. Ligation products were transformed into *E. coli*, yielding 11 colonies on LB+Km agar inoculated with 100 µL of the electroporated suspension after over-night incubation, while transformation of *P. putida* with the same mixture only resulted in one putative colony out of two LB+Km agar plates each inoculated with 100 µL of the electroporated suspension. The putative colony was re-streaked on a fresh plate, but no growth could be observed.

On electroporating *E. coli* cells with ligation products, the time constant was 5.0 ms, which is at the recommended range for electroporation. On the other hand, the time constant when electroporating *P. putida* was only 3.6 ms. During the same experiment, *E. coli* cells had also been transformed with the empty pSEVA258, forming numerous colonies in LB+Km after electroporation had happened with a time constant of 5.8 ms. Based on these observations, it was hypothesized that the lack of *P. putida* transformants was due to low efficiency of ligation or to incomplete removal of salts while preparing electrocompetent cells, the latter resulting in the low time constant for electroporation of *P. putida*.

The higher number of clones from *E. coli* BL21 (DE3) transformed with empty pSEVA258 compared to the transformation with ligation products, on the other hand, would support the hypothesis of low ligation efficiency. It should be noted that, in preparing electrocompentent cells of *P. putida*, the final volume was often more than the prescribed 100 µL from a given culture due to incomplete removal of the supernatant after each centrifugation step. This has likely led to the carry-over of salts from the LB (Miller) medium, resulting in the electroporation suspension having an excessively high conductance made manifest by the low time constant value. Electroporation of *P. putida* with empty pSEVA258 failed due to arcing and nearly complete loss of the cell suspension from the electroporation cuvette. As no more cryo-stocks of electrocompetent *P. putida* were available at the time, it was decided to only transform with the assembled expression vector.

New ligations were made with different insert:vector molar ratios and increased ligation time (from 10 minutes to 1 h at room temperature) but irrespective of insert:vector molar ratios, and despite the longer incubation time, imaging of the agarose gel loaded with the ligation products still showed multiple bands. Then, purification of the assembled plasmid from agarose gel was attempted using the Gel and PCR clean-

up kit from Macherey-Nagel, but the concentration of DNA in the eluate was too low for any practical use. Of note, this problem was encountered by other researchers in the same laboratory when using the same brand of kit.

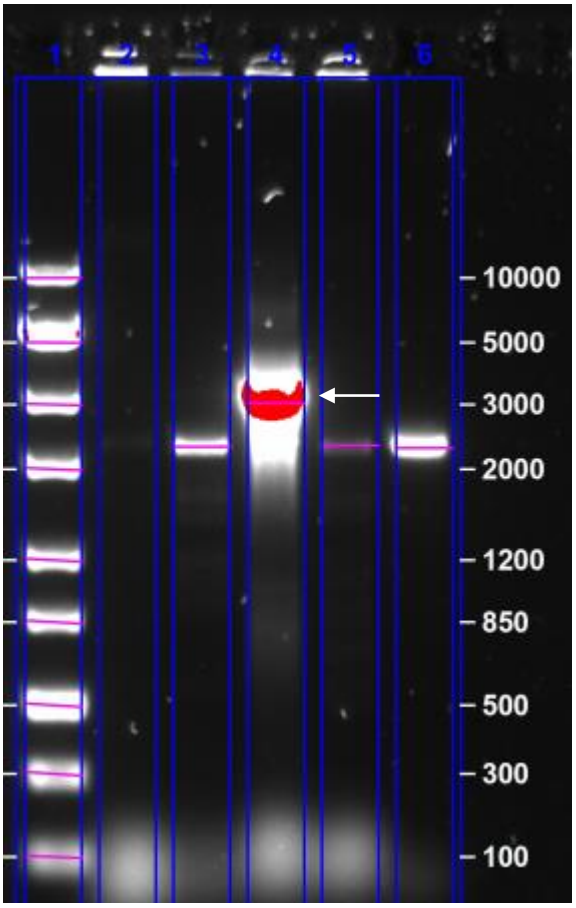

Fig. 2 Agarose gel electrophoresis of colony PCR products from transformants of P. putida. Lane 1: ZipRuler ladder 1. Lanes 2 to 5: colony PCR products. Lane 6: no template control, showing the same band as two of the colony PCR products. The white arrow indicates the amplified insert in pSEVA258.

In parallel to this, the suspension of electroporated *P. putida* cells, which was stored at 4 °C after inoculation of the first two LB+Km agar plates, was centrifuged and the supernatant aspirated to reduce the volume to about 100 µL. The concentrated suspension was then pipetted on a fresh LB+Km agar plate. After overnight incubation, four colonies were observed, which were in turn re-streaked on fresh LB+Km. All four colonies produced biomass on the selective agar, and part of the biomass from each colony was used to provide the template for colony PCR and the inoculum for a cetrimide agar plate. Growth on cetrimide agar was confirmed for all four clones, identifying them as *Pseudomonas* sp. Agarose gel electrophoresis of colony PCR products (Fig. 2) could only confirm one of the colonies as carrying the correct assembly.

A fresh LB+Km agar plate was inoculated with a colony from the successful clone. After overnight incubation, a lawn of cells had formed on top of the agar. Part of the lawn of cells was picked with an inoculation loop and the biomass was resuspended in 300 mM sucrose to make cryostocks (stored at -80 °C). The rest of the biomass was harvested from the plate with minimal salt medium supplemented with Km but no C source. This suspension was kept at 4 °C as a source of inocula for subsequent experiments.

The suspension stored at 4 °C was used as the source of inoculum for an overnight culture from which plasmid DNA was purified. In parallel to this, one of the cryostocks was also used as a source of inoculum for the same procedure. The eluates from the mini-prep procedure were then delivered to Eurofins Genomics for Sanger sequencing with primers PS1 and PS2. Complete sequencing of the cargo module of the assembled plasmid failed due to cargo module in the expression vector being too long relative to Sanger sequencing reads.

Even then, the sequences received from Eurofins Genomics perfectly matched (ignoring the mismatches usually observed towards both ends of a read) the xylS CDS and the entire cloned insert for both the plasmid DNA purified from the cryostock and that purified from the suspension kept at 4 °C.

Having confirmed the successful transformation of *P. putida*, the question remains of the much lower transformation efficiency observed for *P. putida* compared to *E. coli*. Electroporation of *Pseudomonas* spp. cells made electrocompetent at room temperature reportedly should lead to higher numbers of successfully transformed clones than what was observed here [Choi et al, 2006; Wirth et al, 2020]. Both hypotheses raised regarding this issue (low ligation efficiency and incomplete preparation of electrocompetent cells) may be true. Having been unable to transform *P. putida* with the empty pSEVA258, meant that it was not possible to estimate the extent to which the low observed transformation efficiency could be attributed to each of the possible causes, but almost certainly a more accurate preparation of *P. putida* for electroporation would have led to better results.

Protein expression studies

First expression study

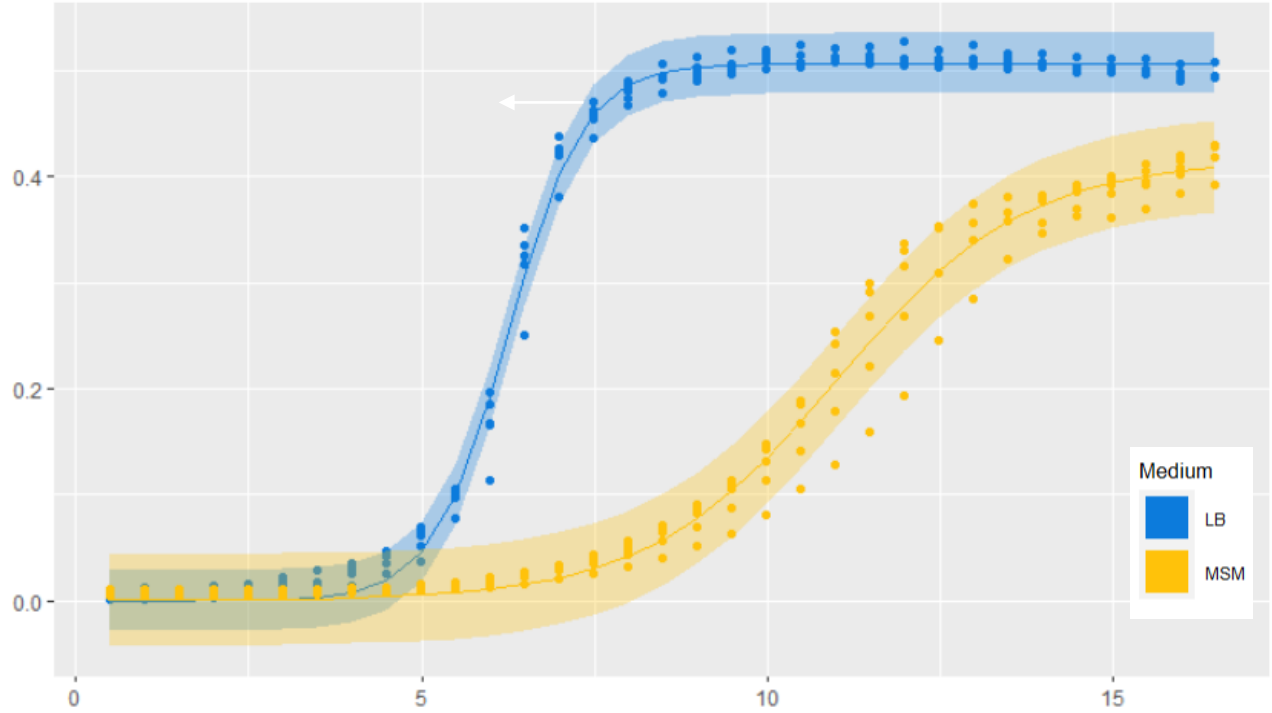

Fig. 3 Growth curves in 12-wells microplates for P. putida 258·SP_{pstu}-$LCC^{ICCG-KRP}$-6XHis in LB+Km and MSM+glucose+Km. The curves fitted to the data are logistic curves. The shaded areas around the curves correspond to 95% confidence interval of prediction.

OD_{600} measured during the first protein expression experiment can be seen in . OD_{600} peaked at 4 h after induction and started to decline afterward. At the 24-hour post-induction mark, suspended solid particles were observed in all cultures. It was initially hypothesized that the suspended particles were 3-mBZ that had precipitated out of the solution due to a reduction in pH, due to a perceived similarity of the particles observed in the culture to undissolved 3-mBZ. The pH of one of the cultures was measured with pH indicator strips covering different ranges, both giving a pH close to 6. As 3-mBZ is dissolved in water at pH 7, this result went towards confirming the initial hypothesis on the nature of the particles observed at 24 h post-induction.

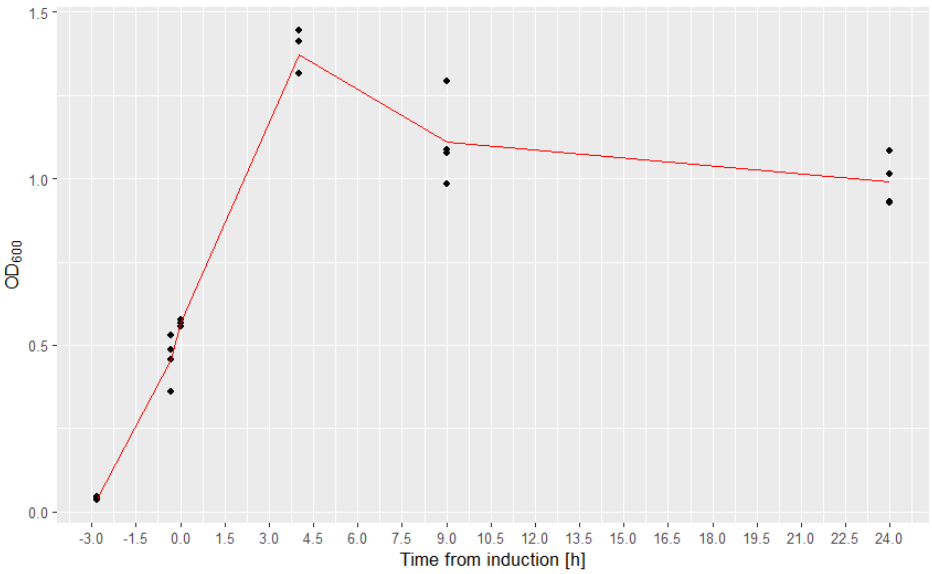

Fig. 4 Plot of OD_{600} versus time for the first induction experiment. The red line describes the average OD at each time point. The 0-hours mark on the x-axis is when 3- mBZ was added to the cultures to 0.5 mM final concentration.

A qualitative esterase assay was performed with the supernatants of one of the cultures. The supernatant of the 0 h post-induction sample showed the most intense yellow colour. As for the other samples, the intensity of the colour seemed to increase with time after induction. This could suggest the successful expression and secretion of LCC, if regarding the intense coloration of the 0 h post-induction sample as resulting from an error. However, the presence of other enzymes in the supernatant of *P. putida* cultures capable of hydrolysing pNPB cannot be ruled out. For instance, a homolog of the EstK esterase was identified in *P. putida* mt-2 and characterized as an extracellular protein and although activity towards pNPB specifically was not assayed, the enzyme was shown to be active in the degradation of other p-nitrophenyl esters [Millar et al, 2016]. A homolog of the same protein was also found in the genome of *P. putida* KT2440.

SDS-PAGE was performed on the samples of one of the four cultures. The SPpstu:LCCICCG-KRP:6XHis-tag fusion has an approximate molecular weight of 31.0 kDa. If the signal peptide is removed, the protein's molecular weight is approximately 28.8 kDa. It was observed in previous studies within our group that, without the addition of DTT to the SDS-PAGE sample buffer, LCC migrates to a band corresponding to about 26 kDa, the longer migration distance due to the presence of disulfide bonds. Analysis by SDS-PAGE of the supernatants sampled during the first protein expression experiment showed no bands corresponding to the above-mentioned molecular weights. It was unclear at this point if the lack of LCC in the supernatant was due to the host cells failing to secrete the protein or to the protein being present at a concentration below the sensitivity of the SDS-PAGE analysis.

It should be noted that the samples taken from the cultures post-induction were all diluted to various extents to maintain the OD_{600} of the samples below values of 0.4 – 0.5, where a linear relationship between cell density and optical density of the culture can be assumed. Moreover, only 20 µL of each supernatant were loaded in the gel. Therefore, secretion of LCC could not yet be ruled out, based on these results.

On the other hand, samples of cell pellets showed a band at roughly 27 kDa after induction of $LCC^{ICCG-KRP}$ expression. The intensity of this band, estimated by the imaging software, increased from 0 h to 4 h post-induction, remained stable in the 4 to 9 h post-induction period, and decreased from there to the end of the experiment. The intensity of the ~27 kDa band in the samples taken after induction was estimated at a higher level than nearby bands, although a more intense band was detected in all cases at around 63 kDa.

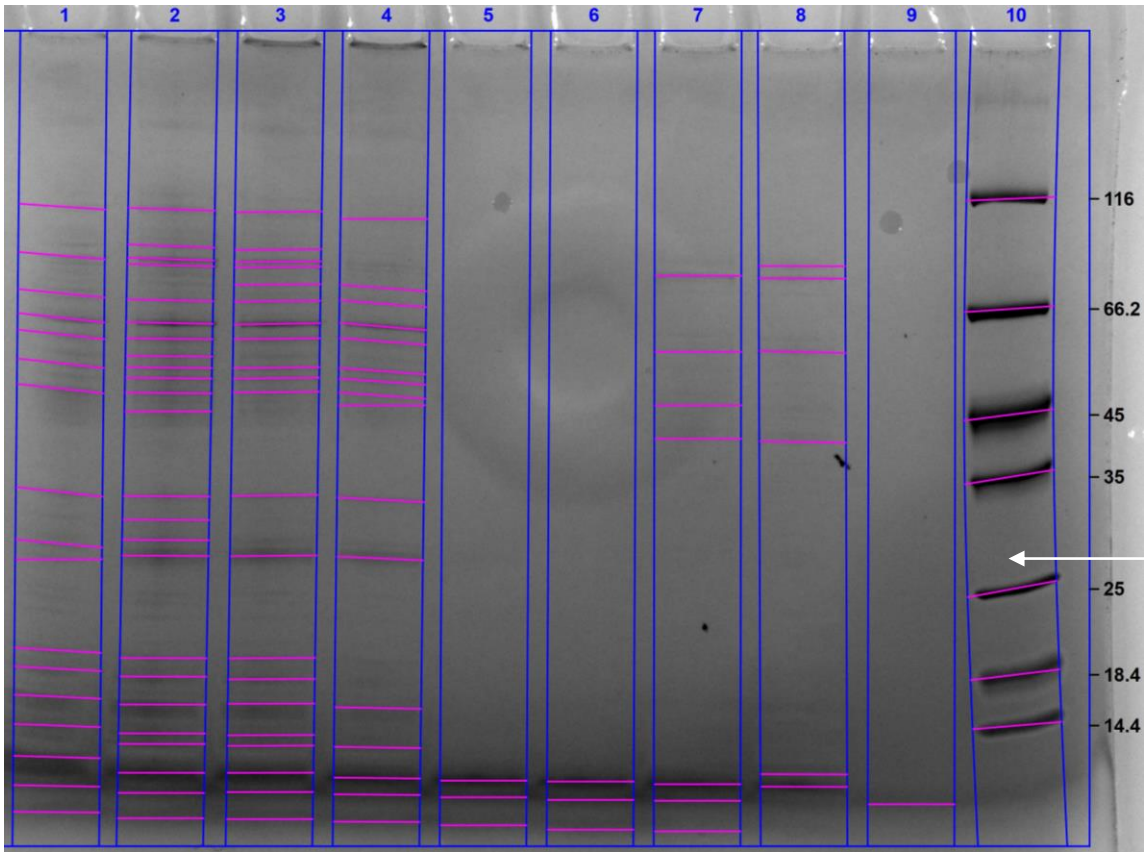

Fig. 5 SDS-PAGE from first expression study. Lanes 1 to 4 loaded with samples of pelleted cells. Lanes 5 to 8 loaded with supernantants. Both supernatants and cells were collected 24 h after induction. Lane 10: Pierce™ marker 26610. The white arrow marks the distance which LCC$^{ICCG-KRP}$ is expected to migrate to.

Identification of the bands from post-induction samples as LCC$^{ICCG-KRP}$, however, would either require use of more specific analytical methods, such as Western blotting or mass spectrometry, or knowledge that no other protein coded for by genes native to *P. putida* KT2440 could have generated the same patterns. Therefore, using the whole genome sequence of *P. putida* KT2440 (GenBank AE015451.2, [Belda et al, 2016]), all amino acids sequences of annotated proteins were extracted, and their molecular weight estimated. 289 proteins have a molecular weight between 25.5 and 28.0 kDa. Most notably among these were enzymes of the Entner-Doudoroff pathway and tricarboxylic acids cycle, such as the gluconate 2-dehydrogenase from locus PP_3384 (26.7 kDa), the fructose-1,6-biphosphatase from locus PP_2871 (27.7 kDa), the 2-ketoglutarate dehydrogenase from locus PP_2652 (27.8 kDa) [Nikel et al, 2015]. Genes that have been found to be upregulated in response to glucose starvation also code for products of a molecular weight around 27 kDa, for instance proC (27.7 kDa), ate (27.9 kDa), the PP_3020 locus (26.9 kDa) [Ankenbauer et al, 2020]. A positive identification of LCC$^{ICCG-KRP}$ in this gel was therefore not possible.

Second expression study

The second protein expression experiment was performed with both the transformed and untransformed strains of *P. putida* KT2440, the hypothesis being that expression of LCC could be identified by comparing the patterns in SDS-PAGE of the two strains.

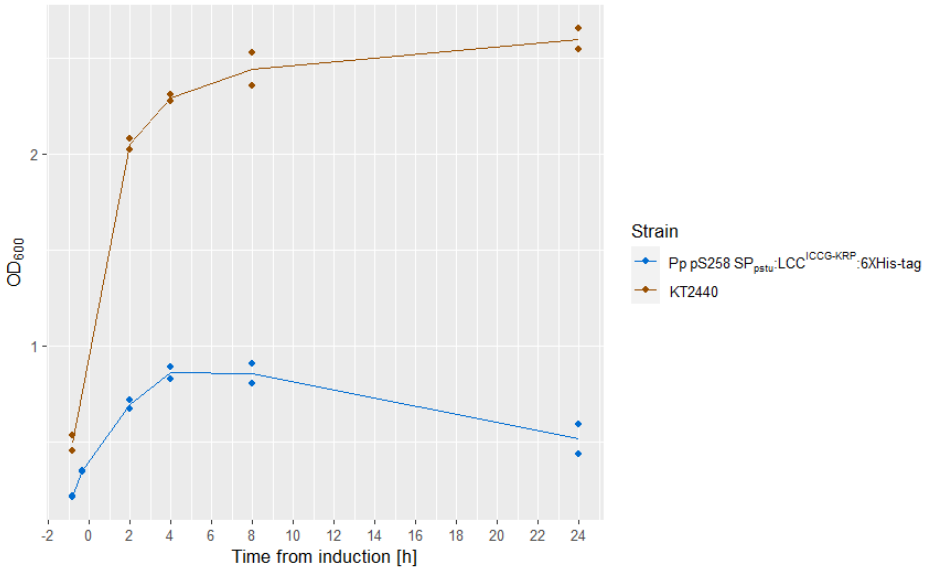

Fig. 6 Plot of OD_{600} versus time for the second induction experiment. The two lines describe the average OD at each time point for each strain. The 0-hours mark on the x-axis is when 3-mBZ was added to the cultures to 0.5 mM final concentration.

Again, the density of cells of the transformed strain peaked at 4 h after induction, decreasing afterwards and especially over the 8 h post-induction mark. On the contrary, growth of the untransformed strain appeared to continue for the entire duration of the experiment, although the measured ODs were too high to be considered accurate and further dilution of the samples would have been necessary. Even with this caveat, it seems reasonable to conclude that the transformant strain was affected by a strong metabolic burden severely straining its ability to grow, at least in MSM with 20 mM glucose.

The presence of suspended particles in the growth medium was again observed at the end of the experiment, but only for the transformed strain. The pH was again measured with pH indicator strips, both in a culture of transformant and in a culture of non-transformant *P. putida*. The pH in the culture of the non-transformant strain turned out to be lower than in the transformant culture, thereby going against the hypothesis that the observed particles were somehow connected to precipitation of 3-mBZ. Later observation of samples of the two strains on a phase-contrast microscope, with and without staining with bromophenol blue, revealed the presence of large aggregates of particles in the transformant culture that would furthermore be strongly stained blue with the dye, indicating that the particles forming the visible aggregates were in fact cells. A report of the clumping of *P. putida* about expression and periplasmic localization of PET-hydrolases, including LCC, can be found in the literature [Brandenberg et al, 2022]. The same paper also reports the appearance of cell lysis, and generally a decrease in OD, past 4 h post-induction, which was also observed in these first two expression experiments, lending credence to the possibility that expression of LCC was indeed happening in our cultures.

Analysing the samples by SDS-PAGE showed again no band that could correspond to $LCC^{ICCG-KRP}$ in the supernatants. The supernatants, especially from 0 h post-induction, showed a high number of bands which probably, given the similarity to cell samples, resulted from the carry-over of cells during collection of the supernatants. It should be noted that, in this second experiment, all cell samples were diluted 1:2 before OD measurements, so the sampled extracellular milieu collected as supernatant of cell pellets was likewise a 1:2 dilution of the culture medium, in contrast to the 3:4 (0 h post-induction samples) and 3:8 dilutions used for the first experiment. Looking at the bands in lanes loaded with samples of cell pellets, there appears to be no clear difference between the profiles of lanes loaded with transformants and non-transformants. The results of SDS-PAGE analysis therefore again failed to support the notion that expression of the GOI cloned in pSEVA258 was working in *P. putida*.

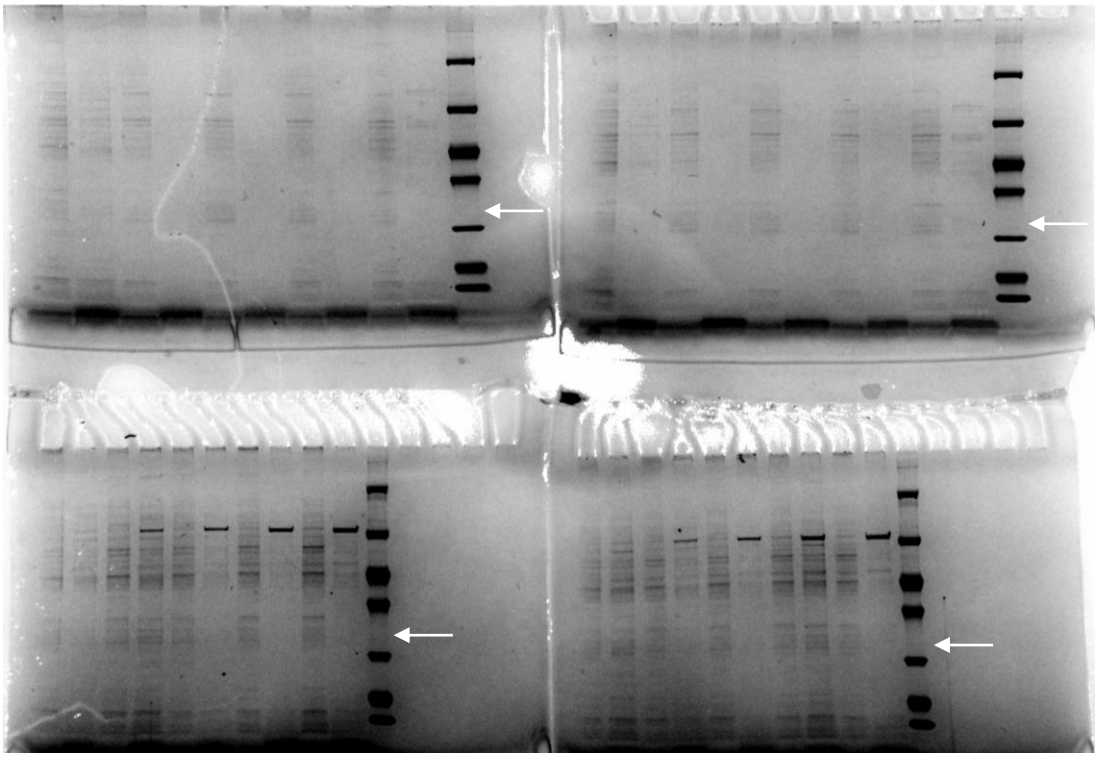

Fig. 7 (previous page) Imaged SDS-PAGE gels from second induction experiment. Top gels loaded with transformants, bottom gels loaded with P. putida KT2440. Order of samples in each gel, left to right is: 0 h pellet, 0 h supernatant, 2 h pellet, 2 h supernatant, 4 h pellet, 4 supernatant, 8 h pellet, 8 h supernatant, 24 h pellet, 24 h supernatant, marker. The white arrows mark the approximate distance that LCC$^{ICCG\text{-}KRP}$ is expected to migrate to.

Third expression study

On the third expression experiment, samples were only taken at 4 and 8 h post-induction. The decline in OD after more than 4 h post-induction could not be confirmed in this study, as the OD measured in the 8 h post-induction samples was higher than what was measured at 4 h post-induction. It is possible that the trend observed in the two previous studies for the transformant *P. putida* was at least in part the result of repeatedly sampling from the same culture while, in this latter case, the entire culture was taken from the incubator at the specified time and analysed.

The values of OD_{600} measured in this study were used as the response variable in two linear models, one per time point, with glucose, $(NH_4)_2SO_4$, and 3-mBZ concentrations as factors. ANOVA was performed with a significance level α of 0.05 on each model using type II sums of squares. At both time points, a statistically significant effect on the response was found for the concentration of the N-source ($b = 0.06$, $\eta^2 = 0.63$, $p = 0.044$ at 4 h post-induction; $b = 0.12$, $\eta^2 = 0.86$, $p = 0.005$ at 8 h post-induction); no other factor had a statistically significant effect on the response. This result would be in accordance with the hypothesis that, after induction, the cells experience a metabolic burden due to gene expression, with increasing concentrations of nitrogen allowing the host organism to better maintain its native cellular machinery in parallel with expression of the heterologous protein.

SDS-PAGE was performed on supernatants from cultures that received treatments other than the centre point of the design due to limited availability of suitable gels. Each well was loaded with 75 µL of supernatant to increase the chances of observing visualising proteins in the gel. A band of slightly more than 26 kDa was found from the supernatants of the cultures harvested 4 h after induction. Out of the samples taken 8 h after induction, only one (20 mM glucose, 4 g/L $(NH_4)_2SO_4$, 0.5 mM 3-mBZ) showed such a band, while the other samples taken at the same time all had bands at 21 kDa and, in one case (40 mM glucose, 2 g/L $(NH_4)_2SO_4$, 0.5 mM 3-mBZ), also a band at 28.7 kDa. All the bands from the supernatants of 8 h post-induction samples were much fainter than most of the 27 kDa bands observed from the 4 h post-

induction samples. This might have been caused by protease activity reducing the size and concentration of the extracellular protein(s) forming the 26 kDa band, but the same pattern was not observable for any other band.

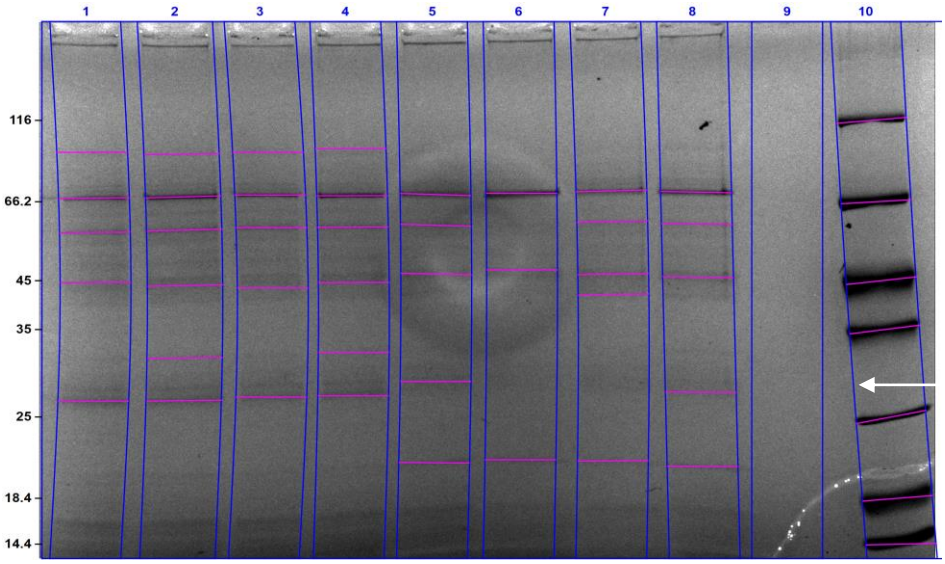

Fig. 8 SDS-PAGE analysis of selected supernatants from third induction experiment. Lanes 1 to 4 are loaded with samples from 4 h post-induction. Lanes 5 to 8 are loaded with samples from 8 h post-induction. Lane 9 was left empty. Lane 10 is loaded with Pierce™ 26610 marker. The white arrow marks the distance which LCC$^{ICCG\text{-}KRP}$ is expected to migrate to.

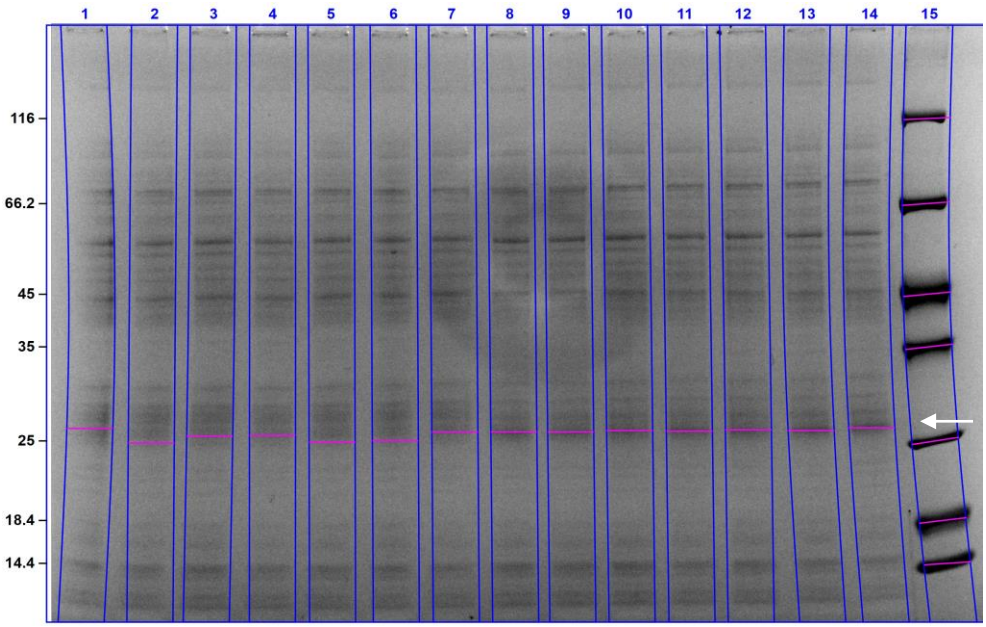

Fig. 9 SDS-PAGE electrophoresis of pelleted cells samples from the third induction experiment. Bands with an estimated size between 24.8 and 26.1 kDa marked. Lanes 1 to 7 loaded with samples from 4 h post-induction. Lanes 8 to 14 loaded with samples from 8 h post-induction. Lane 15 loaded with Pierce™ 26610 marker. The white arrow marks the distance which LCC$^{ICCG\text{-}KRP}$ is expected to migrate to.

On the other hand, the SDS-PAGE analysis of the cell pellets did not show any clear difference between treatments, including here 3 of the 4 centre points of the experimental design, and time from induction to cells harvest. All the samples from pellets showed a band with an estimated molecular weight of between 24.8 and 26.1 kDa, somewhat below the expected size for LCC$^{ICCG\text{-}KRP}$. No conclusive evidence for expression of LCC in *P. putida* could thus be gleaned from this experiment either.

Fourth expression study

The fourth induction experiment was performed with LB (Miller) medium to explore whether the use of a richer growth medium could lead to clearer indications of expression of the GOI. The values of OD_{600} measured on the cultures withdrawn from the incubator at the specified times (0, 2, 4, 8 h post-induction) generally showed no marked difference between the non-transformed and transformed *P. putida* strains. Only the cultures sampled 4 h post-induction showed a large difference in OD between the two strains, with the transformed strain showing a much lower OD than the untransformed strain. Given the small difference in OD observed between the two strains at the end of the experiment, it seems likely that an error occurred in measuring the OD on the culture of transformed *P. putida* withdrawn 4 h post-induction. It would seem from this that there is metabolic burden imposed on the transformed strain by plasmid maintenance and GOI expression, possibly due to higher N concentration and the presence of vitamins in the growth medium supplied by the yeast extract.

Analysis by SDS-PAGE samples of cell pellets and supernatants did not yield additional information compared to previous attempts, with the two strains essentially showing the same patterns of bands. Notably, the preparation of samples of cell pellets with 5 µL of 1 M DTT, followed by SDS-PAGE analysis, was explored as a way to make the migration of proteins through the gel more closely linked to their molecular weight, but no pattern could be seen that would unequivocally indicate the presence of $LCC^{ICCG\text{-}KRP}$ in the sample.

SDS-PAGE analysis was performed on the cells of both strains cultivated in the fourth expression study, with harvested cells from the 0 h and 8 h post-induction cultures in an attempt to verify the presence of inclusion bodies. The samples of resuspended pellets were prepared for SDS-PAGE as done previously, to a volume of 50 µL, up to incubation at 95 °C. Then, instead of loading the denatured samples directly on the gel, they were centrifuged at 10000 g for 5 minutes and a 20 µL aliquot of each was loaded in a well, followed by resuspension of any insoluble material in the remaining volume by pipette-mixing and loading of a second aliquot.

In principle, a band that shows up in the second aliquot of a sample with this method, but not in the first, would suggest that said protein is localized in inclusion bodies. Proteins that were in solution within the cytoplasm or periplasm of the cells should instead generate the same band from both aliquots at the same distance along the gel, while proteins that exist in an equilibrium between the liquid and solid phase should also appear in both aliquots but with a more intense band in the resuspended aliquot.

This analysis was done approximately one month after the cells from the fourth expression experiment were harvested and stored at 4 °C. The pellets were first re-suspended in 10 mL of 50 mM KPO buffer (pH 8.0). Some indications of cell lysis could be seen while resuspending the pellets, with the biomass floating in the buffer as a single, viscous clump. This clump required intense pipette mixing to be broken. The suspensions from the cultures that were incubated until 8 h post-induction showed higher viscosity indicative of the presence of nucleic acids in the solution, itself a sign of cell lysis. The OD_{600} of the suspensions was measured, and variable volumes of each suspension were taken as appropriate to have an OD of 0.2 in the SDS-PAGE solution.

Various bands from both the wild type and from the transformant *P. putida* strain showed a pattern that would be consistent with their presence within inclusion bodies (i.e., higher intensity in the pipette-mixed aliquot of each sample). In most cases, this behaviour was observed in bands from the samples of transformant *P. putida* but not in the corresponding bands of samples of wild type *P. putida*, potentially indicating a connection with the expression of our GOI. However, none of these bands was in the range where $LCC^{ICCG\text{-}KRP}$ was expected to be found.

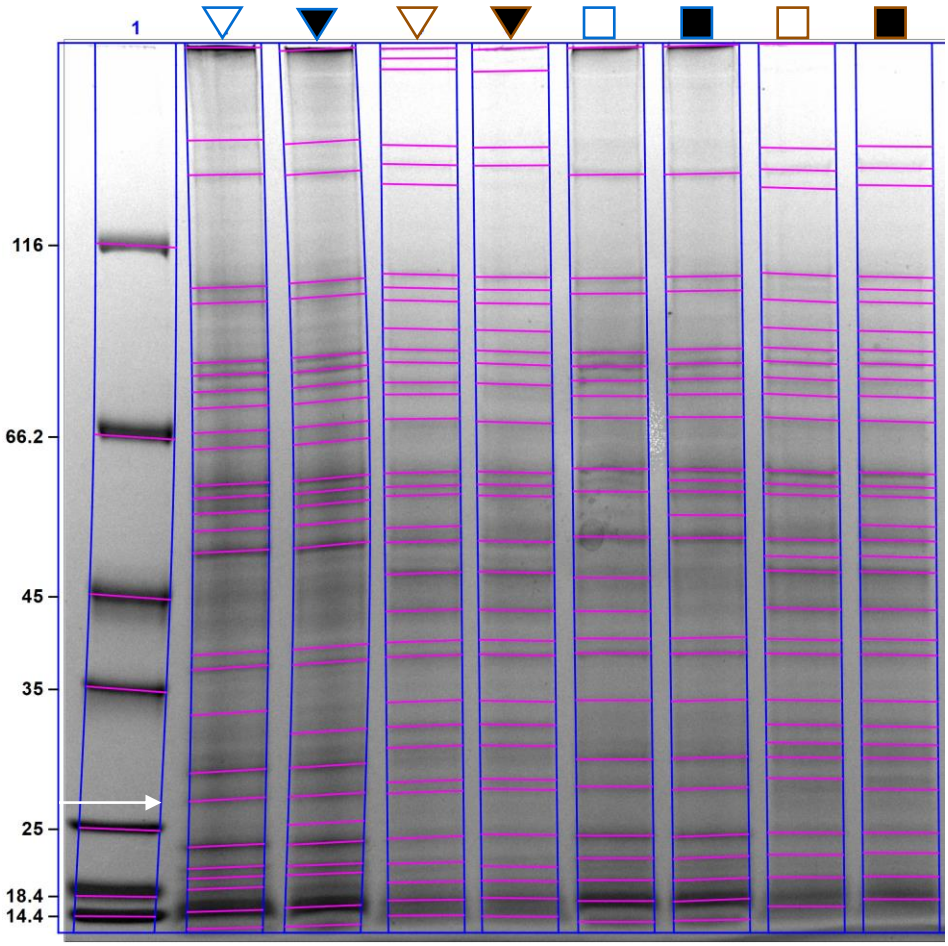

*Fig. 10 SDS-PAGE analysis of cell pellets from the fourth expression study to assess the presence of inclusion bodies. Lane 1: PierceTM marker 26610. Lanes marked with triangles were loaded with P. putida KT2440. Lanes marked with squares were loaded with transformant P. putida. Empty shapes correspond to lanes loaded with centrifuged aliquots of samples, filled shapes were loaded with resuspended aliquots. --: 0 h post-induction. --: 8 h post-induction. Note: the original gel image includes three more wells on the right side, from a different experiment, cropped in this image for readability (see **Error! Reference source not found.**). The white arrow marks the distance which LCC$^{ICCG-KRP}$ is expected to migrate to.*

Interpretation of gel bands was also complicated by the distortion of, especially, the lateral bands, making molecular weight and intensity analysis of the bands more difficult fo the imaging software. In addition to this, the samples of cultures taken from the incubator at 0 h post-incubation presented thick bands of Coomassie stain at the bottom of the wells (upper margin of **Error! Reference source not found.**), meaning that a part of the proteins in those samples likely failed to migrate through the gel. Lastly, it is possible that inclusion bodies were not entirely removed from suspension due to excessively short duration of the centrifugation, with much longer centrifugation times reported for inclusion bodies purification from cell lysates [Zhang et al, 2018].

In conclusion, the protein expression studies presented herein gave cursory evidence of the existence of a metabolic burden experienced by *P. putida* 258·SP$_{pstu}$:LCC$^{ICCG-KRP}$:6XHis after induction, which may be indicative of expression of the GOI. The presence of LCC$^{ICCG-KRP}$ could not however be clearly identified from SDS-PAGE analyses, neither in culture supernatants nor in cells.

Purification of LCC$^{ICCG-KRP}$

Results of SDS-PAGE analysis for the first IMAC purification of LCC$^{ICCG-KRP}$, performed on the pooled cells harvested 24 h after induction, are shown in **Error! Reference source not found.**. The most notable result is the presence, in the second and third fractions of the eluate, of a single band with an estimated molecular weight of 27.4, in line with what was expected for LCC$^{ICC-KRP}$. Bands of corresponding size can also be observed in the cell lysate, flowthrough (with much lower intensity than in the cell lysate), and column

wash samples, but not in the first eluate fraction. The faintness of the bands observed in the eluates compared to the corresponding bands in the other samples suggests that LCC$^{ICCG-KRP}$ is expressed at very low levels, which would be in line with the observed similarity in lane profiles for samples from wild-type *P. putida* and from the transformant strain.

It might also be possible that the protein did not bind effectively to the column's stationary phase. Likely due to an error during preparation, the binding buffer had a very low electrical conductivity as measured by the instrument's on-line conductometer. The presence of a salt in the buffers serves to reduce non-specific binding to the column [Bornhorst & Falke, 2000], and excessive binding of non-tagged proteins might have reduced the available capacity of the column for the His-tagged protein. The profile of the lane loaded with the column wash, however, goes against this hypothesis, as the most prominent band is aligned with the 27.4 kDa bands in the eluate, suggesting that most of the non-tagged proteins did not bind to the column.

That the His-tagged LCC$^{ICCG-KRP}$ itself overcame the capacity of the column also seems unlikely, as the manufacturer of the column reports 40 mg/mL of buffer as the minimum column binding capacity for a pure His-tagged protein. Quantification of proteins by the Pierce™ Bradford assay in the various liquid phases recovered from the column resulted in estimates of 29.6, 7.4, 13.2, 10.7 µg/mL for the wash, first eluate, second eluate, and third eluate, respectively. Unless the column's capacity had been reduced by previous uses, through loss of the nickel ions in the stationary phase, these concentrations are well below the capacity of the column.

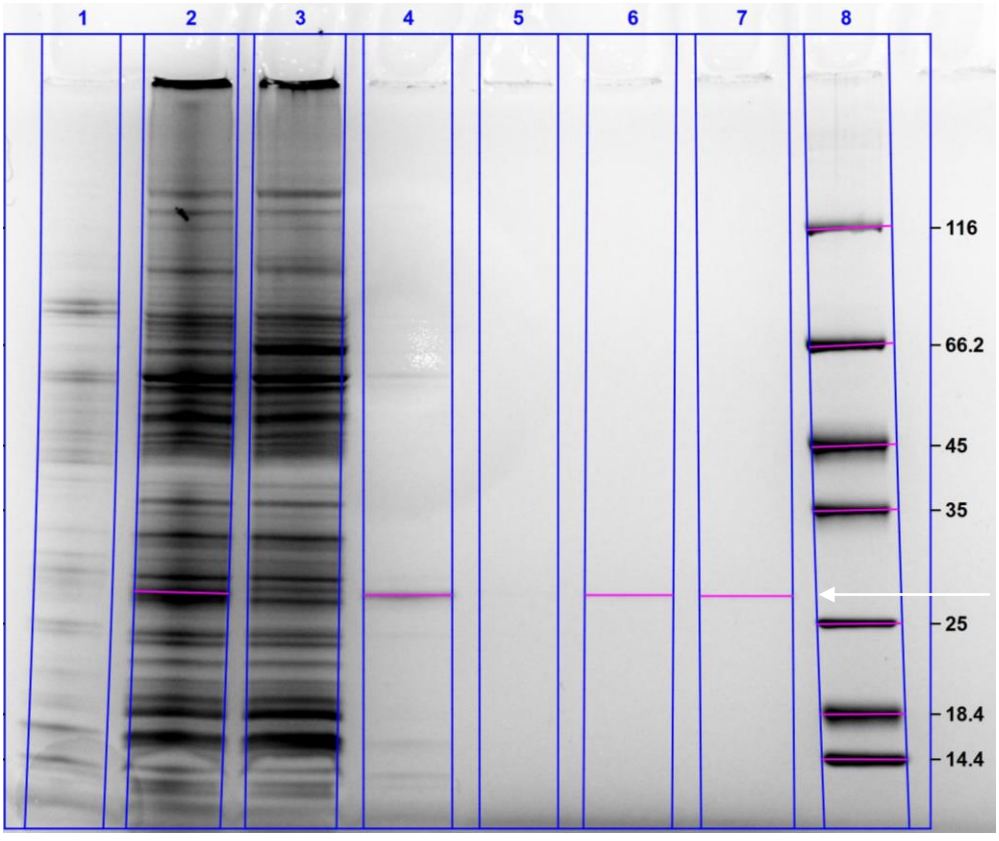

Fig. 11 SDS-PAGE of fractions from IMAC purification of intracellular LCC$^{ICCG-KRP}$ from first expression study. From left to right, lanes loaded with: cells supernatant, clarified lysate, sample flowthrough, column wash, elution fraction 1, elution fraction 2, elution fraction 3, marker Pierce™ 26610. The white arrow marks the distance which LCC$^{ICCG-KRP}$ is expected to migrate to.

Something worth noticing is that the column wash was itself highly pure, with the most intense band corresponding to a molecular mass of 27.2 kDa, and much fainter bands located elsewhere along the lane. It seems unlikely that the only non-tagged proteins capable of non-specific binding on the column would be

ones of a similar size as the His-tagged protein. A more reasonable assumption would be that the His-tagged protein failed to bind to the column. This could happen due to the protein being within inclusion bodies, making the His-tag unavailable for binding to metal ions. However, none of the methods employed for solubilisation of inclusion bodies was used here [Singh et al, 2015], cell lysis buffer being the same solution used as binding buffer for IMAC. Furthermore, clarification of the lysate was performed by centrifugation at 2540 g for 30 minutes, followed by collection of the supernatant, which was visibly clear at this point, in a separate container. Given the reportedly higher density of inclusion bodies compared to cell debris [Georgiou & Valax, 1999] (albeit with differences among inclusion bodies of different proteins [Taylor et al, 1986]), the centrifugation conditions used should have also removed inclusion bodies from the lysate.

Another possibility would be that, due to the particular folding conformation of the protein, the His-tag is not well exposed to the solvent, limiting the ability of the tag for binding to the column.

The second run of purification of $LCC^{ICCG\text{-}KRP}$ by IMAC showed slightly different behaviour, probably on account of batch-to-batch differences in the formulation of the buffers, and the different way the chromatographer was operated. That said, results for the two sets of cultures used as source of cells (4 and 8 h after induction, from the third expression study), showed similar patterns when the liquid phases recovered from the chromatographer were analysed by SDS-PAGE.

First, the cell lysates showed a thick band at about 27 kDa, which could suggest the presence of $LCC^{ICCG\text{-}KRP}$ in the cells, in which case the chemical lysis protocol would be proven to not be effective at extracting the full amount of the expressed enzyme from the biomass. Research on the chemical lysis buffer that was used here suggests that the cell membranes are not completely dissolved, instead their permeability is increased by Triton X-100 [Danilevich et al, 2006]. It is not clear if this effect applies equally to the outer and inner membrane. If this was not the case, the aforementioned bands would mean that localisation of our fusion protein to the periplasm is not efficient, potentially with the concurrent formation of inclusion bodies.

Compared to the observations of the first IMAC purification, the second one resulted in lower purity of the His-tagged protein in the eluates, with the first two fractions showing multiple bands for both purification runs. The presence of additional proteins in the eluates of the second IMAC could have simply been caused by usage of a smaller volume of wash buffer compared to the first purification, although a comparison is not possible to having used an unspecified volume of wash buffer on the first run, when the move to the elution buffer was instead based on observing the UV absorbance downstream of the column.

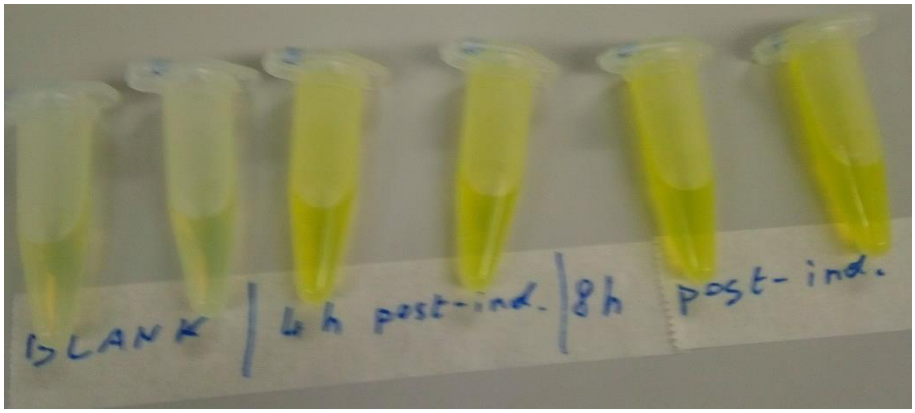

Fig. 12 Quantitative esterase assay with retentates from diafiltration of second IMAC eluates.

The 3rd and 4th fractions of the eluates showed two bands instead of the one observable from the gel of the first IMAC. The two bands differ in their estimated molecular weights by approximately 2 kDa, which is in good agreement with the molecular weight of the signal peptide, thus indicating that both the cytoplasmic and periplasmic fraction of $LCC^{ICCG\text{-}KRP}$ were loaded on the column. Besides differences in the resolution of the two SDS-PAGE analyses, the presence of only one band identifiable with $LCC^{ICCG\text{-}KRP}$ in the eluates of the

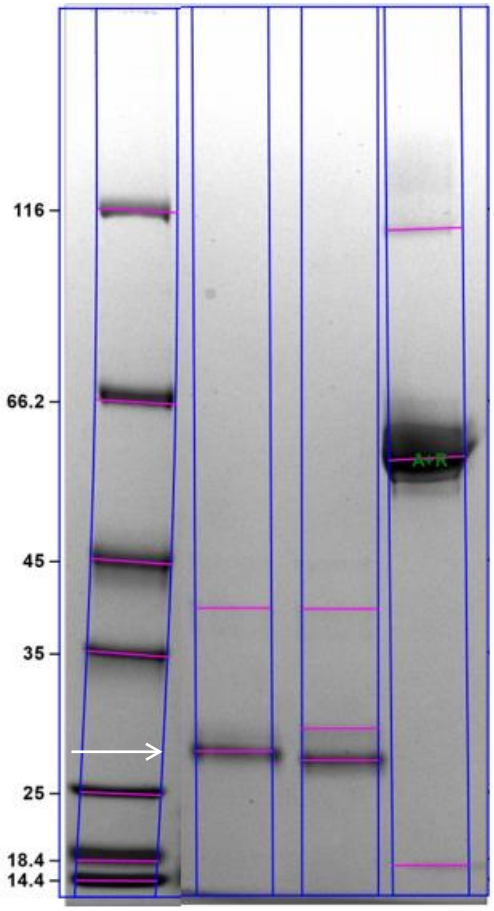

Fig. 13 SDS-PAGE analysis of retentates from diafiltration of LCCICCG-KRP (lanes 2 and 3) and BSA standard (lane 4). PierceTM marker 26610 in first lane. Original picture included the other wells from Fig. 8. The white arrow marks the distance which LCC$^{ICCG-KRP}$ is expected to migrate to. The white arrow marks the distance which LCC$^{ICCG-KRP}$ is expected to migrate to.

first IMAC purification was probably due to the chemical lysis buffer containing Triton X-100. This, like other mild detergents, can solubilise proteins from inclusion bodies [Jevševar et al, 2005; Ryan & Kinsella, 2017] and thus, if LCC$^{ICCG-KRP}$ indeed formed inclusion bodies in *P. putida*, presence of the detergent would therefore lead to the appearance on gel of the cytoplasmic fraction of LCC$^{ICCG-KRP}$, still fused to the signal peptide, in the second IMAC.

The 3rd and 4th elution fractions from the second IMAC were then pooled together based on originating culture and ran through diafiltration. The final retentates appeared somewhat viscous, and no protein concentration could be measured by either NanodDrop or Pierce^{TM} Bradford tube assay. However, a qualitative esterase assay revealed strong esterase activity in both retentates (Fig. 12).

It was then hypothesised that LCC$^{ICCG-KRP}$ had either precipitated in the filtration unit due to its increased concentration, or that it had adsorbed on the filter. An attempt was made at re-solubilising the protein from the filtration units using 50 mM KPO buffer (pH 8.0) with 100 mM NaCl, but no significant improvement on mixing samples of the retentate with Bradford reagent could be seen.

It was later decided to perform SDS-PAGE analysis on the retentates and on a 250 µL/mL bovine serum albumin (BSA) standard that was also used for calibration of Bradford tube assays, using the intensity of the BSA band as a standard to estimate the amount of proteins in the retentates on the gel imaging software. The retentates appeared mostly as single bands, although the amount of protein loaded in the wells may have resulted in excessively large bands and a loss of resolution compared to what was seen from SDS-PAGE of the IMAC eluates. The estimated amounts were 458 and 450 ng in the two retentates, which translates to concentrations of LCC$^{ICCG-KRP}$ in the two retentates of 24.4 and 24.0 µg/mL. A Bradford micro-tube assay on one of the retentates confirmed this estimate.

The concentration of proteins in the eluates ran through diafiltration were estimated by Bradford micro-tube assay as 15.8 and 15.1 µg/mL. Given this, an initial volume of circa 10.2 mL for each pooled eluate, and final volumes of between 0.5 and 0.8 mL for the retentates, the concentration of LCC$^{ICCG-KRP}$ after diafiltration should have been in the range 192 to 322 µg/mL, indicating a significant loss of protein in the filtration units which probably has to do with the hydrophobicity of LCC$^{ICGG-KRP}$.

PET depolymerisation assays

The eluates and column wash of the first IMAC were used to run PET depolymerisation assays in triplicates, with a blank (only KPO buffer) and culture supernatant of wild type *P. putida* KT2440 from the second expression study used as controls. The culture supernatant from the first expression study was also used as treatment. All treatments and blanks were run in triplicates.

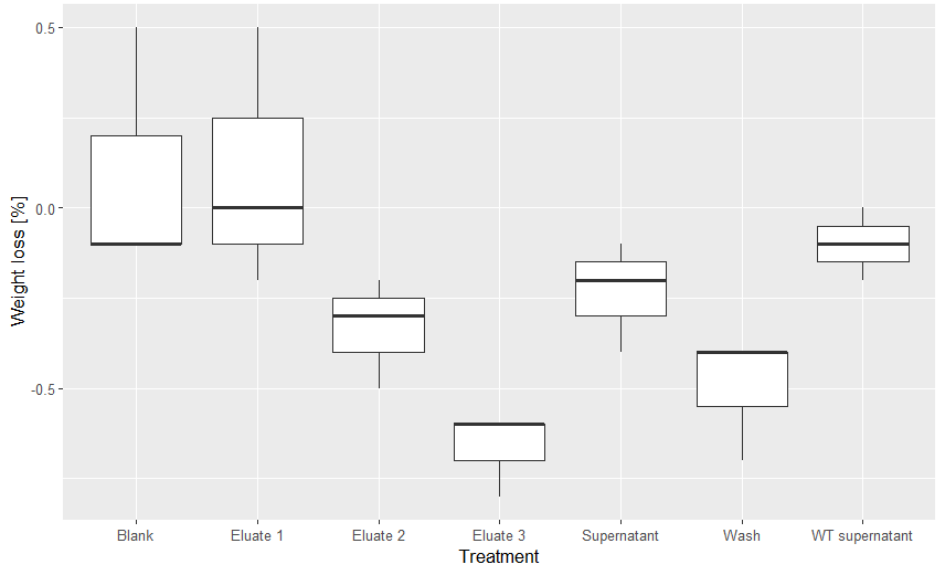

Fig. 14 Boxplot of the first PET depolymerisation experiment, showing weight loss as a percentage of the initial weight for each treatment. Treatments were applied in triplicates.

Results from a Bradford micro-tube assay were used to normalise the concentration of proteins in the various treatments using the molecular weight of $LCC^{ICCG\text{-}KRP}$ minus the SP to covert mass concentrations to molar concentrations (in other words, assuming only $LCC^{ICCG\text{-}KRP}$ was present in the samples). In part due to the very low concentrations of proteins in all the sampled solutions, in part due to a computational error, the actual concentration of $LCC^{ICCG\text{-}KRP}$ in the eluates was 0.006 µM, instead of the prescribed 5 µM.

The average weight loss, in percentage of the starting weight, and 95% confidence intervals for each treatment are shown in Fig. 14. Even though the

concentration of enzyme was 1:1000 the standard concentration for the assay, a statistically significant weight loss (C.I.'s not encompassing zero) could be detected from the 2nd and 3rd fractions of the eluate. Statistically significant weight loss was also found for the column wash, confirming that a large part of $LCC^{ICCG\text{-}KRP}$ had co-eluted with non-tagged proteins. A better approach to IMAC in this case might have been a two-buffers protocol, with column wash done with the binding buffer with 5 mM imidazole, followed by elution with a larger volume 200 mM imidazole buffer, aiming for non-tagged proteins to be collected, at most, in the first fraction of eluate. Most interestingly, even though $LCC^{ICCG\text{-}KRP}$ could not be identified in SDS-PAGE analyses of the supernatant, a statistically significant weight loss was also found for the culture supernatant.

A second PET depolymerisation experiment was run with the retentates from the diafiltration tubes. Since this was set up before the concentration of enzyme could be estimated with the Bradford micro-tube assay, the reaction mixtures were prepared with 100 µL of each retentate. Given the estimated concentrations of 24.4 and 24.0 µg/mL, the reactions were therefore prepared with a final concentration of enzyme of approximately 0.08 µM, or circa 14 times the concentration of enzyme in the first assay.

The results are shown in a boxplot in Fig. 15**Error! Reference source not found.**. Statistically significant weight losses, much larger than anything measured from the first assay, were found for both retentates (averages of -23.6% and -17.1%). The difference in average weight loss between reactions carried out with the two retentates should not be overinterpreted: even though care had been taken with cutting the PET film into pieces of the roughly the same size, there was still some variance in the weights of PET film fragments, and the initial weights of film used in the reactions with enzymes from 4 h induction being on average lower than they were for the reactions with 8 h induction enzymes. Indeed, in this second depolymerisation experiment, there was a strong correlation between the initial weight of a PET film and

the corresponding weight loss (r = 0.92). It is likely that lighter, therefore smaller, pieces of film have a higher ratio of possible enzyme binding site per unit of volume, therefore leading to higher depolymerisation rates, all else held constant.

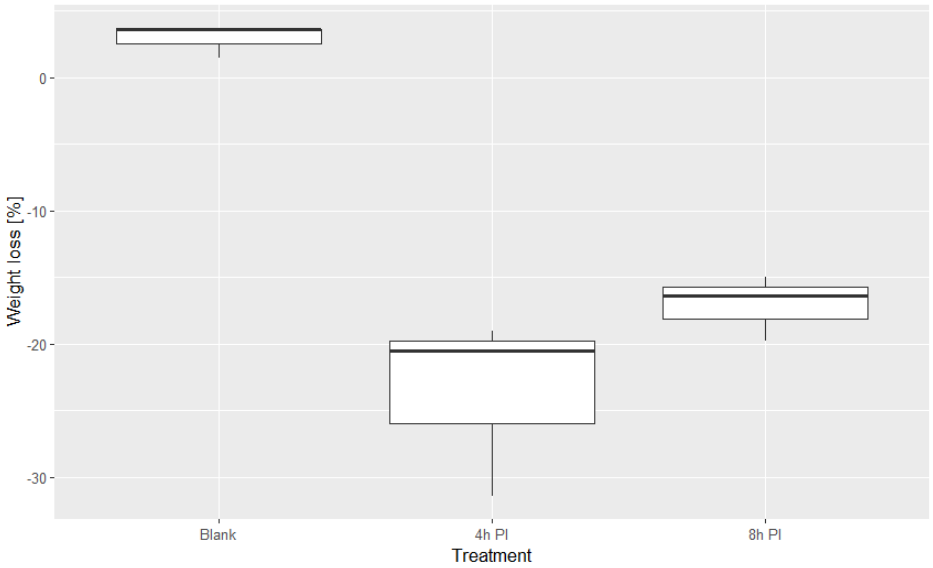

Fig. 15 Boxplot of the second PET depolymerisation experiment, showing weight loss as a percentage of the initial weight for each treatment. Treatments were applied in triplicates.

In other studies, conducted within our group, complete depolymerisation of PET films could be observed after 24 h when the plastic was incubated with LCC$^{ICCG\text{-}KRP}$ expressed in *E. coli* BL21 (DE3). Are then the lower ratios of depolymerisation observed in these two assays due to expression in *P. putida* causing alterations to the structure of the enzyme, or due to the concentrations of enzyme being lower than the prescribed 5 µM for the standard depolymerisation assay?

In the studies with enzymes expressed in *E. coli*, 13 mg of PET film were converted in 24 h to 56 mM terephthalic acid, with no visible film in the reaction mixture, and the depolymerisation assumed to have been complete; no significant amounts of MHET or BHET were detected and the mass of terephthalic acid produced in the enzymatic reaction accounted for 72% of the initial mass of PET. One definition of the specific activity of a PET depolymerase is $mg_{Taeq}\ h^{-1} mg_E^{-1}$ [Tournier et al, 2020], where mg_{TAeq} is the mass of terephthalic acid equivalents (sum of free TA and TA found in MHET and BHET) estimated from the reaction products and mg_E is the mass of enzyme used in the reaction. Therefore, the specific activity of the LCC$^{ICCG\text{-}KRP}$ expressed in *E. coli* would be 13.54 $mg_{TAeq}\ h^{-1}\ mg_E^{-1}$, with a concentration of enzyme of 1 µM, corresponding to 28.8 $\mu g\ mL^{-1}$.

The enzyme specific activity in the reaction mixes of the second PET depolymerisation assay can then be estimated as:

$$SA = \left(m_{PET,i} - m_{PET,f}\right) * 0.72 * t^{-1} * m_E^{-1}$$

where SA is the specific activity, $m_{PET,i}$ and $m_{PET,f}$ are the initial and final mass of PET film in mg, respectively, t is the duration of the assay in hours, m_E is the mass of enzyme in the reaction mix in mg. With this formula, the specific activity for LCC$^{ICCG\text{-}KRP}$ produced in 4 h induction is estimated to have an average and standard deviation of 11.75±1.55, while for the 8 h induction the average and standard deviation are 10.28±0.24 $mg_{TAeq}\ h^{-1}\ mg_E^{-1}$. The values for LCC$^{ICCG\text{-}KRP}$ expressed in *P. putida* are therefore close to what was observed with *E. coli*. Considering the lower concentrations of enzyme and that the specific activity was estimated based only on the end-point of a 72 h-long incubation, with no way of saying if the reaction had stopped any earlier, from a qualitative point of view, LCC$^{ICCG\text{-}KRP}$ expressed in *P. putida* appears to be comparable to that expressed in *E. coli*.

Qualitatively, the picture is more muddled, given the large uncertainty with identifying expressed $LCC^{ICCG-KRP}$ in *P. putida* based solely on SDS-PAGE, and the potential localisation of the enzyme within inclusion bodies. What is clearer is that the secretion of the enzyme by *P. putida* has effectively failed, with very low concentrations of extracellular proteins in general, and more specifically very weak bands in SDS-PAGE that could be suspected of being $LCC^{ICCG-KRP}$.

It was also hypothesized that the low observable expression of $LCC^{ICCG-KRP}$ could be due to a low compatibility of the RBS cloned to pSEVA258 from the pET28a(+) backbone and *P. putida*. However, the same sequence (AAGGAG) was shared by the RBSs observed as resulting in the strongest expression of GFP in *P. putida* [Aparicio et al, 2020; Cook et al, 2021].

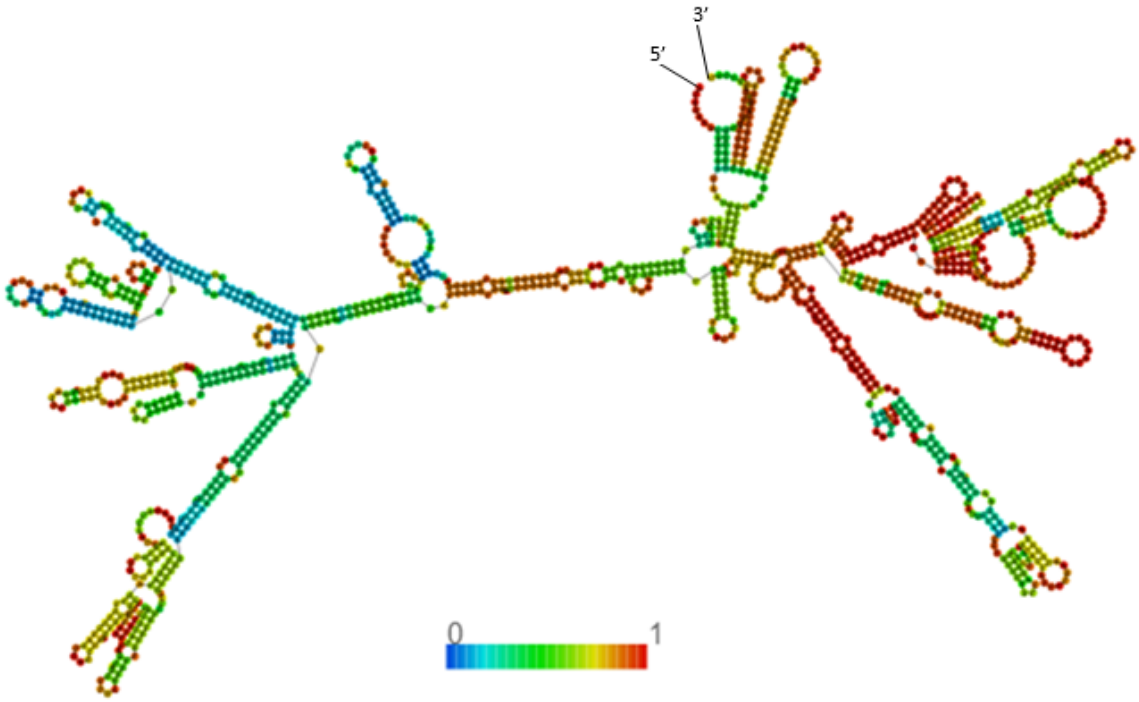

Fig. 16 Minimum free energy structure predicted by RNAfold for the mRNA transcribed from within the Pm->T0 region of the expression vector. Nucleotides are coloured by base pairing probability. The 5'- and 3'-ends of the mRNA are indicated on the picture.

Next, the distance between the transcription start site (TSS) of the *Pm* promoter and the start codon of the GOI (corresponding to the leader sequence) was evaluated as a potential cause for the apparent low protein expression. Said distance is 117 bp, which is below the 136 bp median length for leader sequences found in the genome of *P. putida* KT2440 [D'Arrigo et al, 2016], thus the length of the leader sequence upstream of the GOI does not appear to be a major concern.

The DNA sequence of the expression vector between the TSS of the *Pm* promoter and the T0 terminator was transcribed *in silico* and the resulting mRNA sequence was submitted to University of Vienna's RNAfold web server for prediction of the secondary structure in order to verify the presence of stem loops that could lead to premature transcription termination [Gruber et al, 2008] (Fig. 16). While multiple stem loops with high base-pairing probabilities were predicted in addition to the stem loop formed by nucleotides in the T0 terminator, none of them had a U-rich sequence on or near their 3'-end as required for rho-independent transcription termination.

The near complete absence of secretion of proteins (secretion being the release of a compound outside the cell, not merely in the periplasm) that are expressed in fusion to Sec- or Tat-dependent SPs is not unprecedented when looking at the relevant literature [Filloux, 2022]. The most well-known mechanism for secretion of periplasmic proteins are the type 2 and type 5 secretion systems. T5 secretion systems, also

called autotransporter systems, are composed of a β-barrel domain that integrates itself in the outer membrane and provides a passage through the outer membrane for the passenger domain, which includes the catalytic site of the whole protein. A linker can usually be identified, holding the two domains together and allowing the passenger domain to enter the β-barrel domain and being exposed to the extracellular milieu [Burdette et al, 2018]. The main disadvantage of this system with PET-depolymerising enzymes, is that disulfide bonds on the passenger domain severely constrains T5SS secretion [Leyton et al, 2011]. The T2SS on the other hand is a complex machine that spans the internal and outer membrane and actively transports proteins through the outer membrane. The mechanism by which T2SS's recognize their substrates is presently unknown. It is not the N-terminal signal peptide such as we have been fusing to our proteins of interest, as substrates of T2SS have their signal peptide cleaved by signal peptidases when the protein is translocated to the periplasm, and it is thus not available to interact with the T2SS [Korotkov & Sandkvist, 2019]. In general, substrate recognition by the T2SS appears to be species specific or even strain specific to the point where secretion of heterologous proteins without any domain from secreted native proteins is unlikely to result in secretion of the heterologous protein (Filloux, 2004; Korotkov et al, 2012).

There are indications that different T2SS's in the genome of a given bacterial strain only recognise each a different subset of T2SS secreted proteins. In *Pseudomonas putida*, two type 2 secretion systems have been identified. One includes the putative phosphatases UxpA and UxpB, the secretion of which has been linked to low Pi concentration as a necessary condition to elicit expression not just of the phosphatases but of the T2SS as well (Putker et al, 2013). The other type 2 secretion system in *Pseudomonas putida* has been linked to the secretion of a manganese multicopper oxidase (De Vrind et al, 2003).

There are reports of protein secretion through localization to the periplasm in *E. coli*, for instance, using the PelB signal peptide and enhanced versions of it to secrete IsPETase [Cui et al, 2021]. Reportedly, the signal enhancer improved secretion from the periplasm but this goes against evidence that the signal peptide of PelB is cleaved in *E. coli* in the context of translocation [Mirzadeh et al, 2020].

The most probable way for heterologous proteins to move from the periplasm to the extracellular milieu is thus through damaged regions of the outer membrane, with the damaged resulting from the overexpressed protein's activity or just by the accumulation of the protein. Expression and localisation to the periplasm in *E. coli* of the cutinase from *Thermobifida fusca* was observed to lead to the release of the enzyme to the growth medium, with the morphology of the cells, when observed by TEM, visibly altered compared to wild type cells, while an assay for β-galactosidase, an otherwise cytoplasmic enzyme, gave a positive result when performed on the culture supernatant [Su et al, 2013].

Future perspectives

One of the original objectives of this project, i.e. the quantitative description of PET-depolymerising enzymes expression and secretion if *P. putida*, could not be completed in time. The question therefore remains open as a prerequisite for an informed evaluation of the enzymes' production process ahead of commercial deployment.

A question raised by this project regards the localisation of $LCC^{ICCG\text{-}KRP}$ within the cells of *P. putida*, particularly whether or not the protein forms inclusion bodies. To answer this, SDS-PAGE would have to be complemented by Western blotting to eliminate any uncertainty about the identity of the bands observed in SDS-PAGE analyses.

The presence of inclusion bodies in the cells might be indicative of protein synthesis overcoming the capacity of the cytoplasmic protein folding machinery or the translocation pathway. With regards to the latter, the SP used in this project is recognised by the Sec pathway. Whereas translocation through the Sec pathway requires one unit of ATP per unit of protein transported through the membrane, translocation by the Tat pathway is reported to be exclusively associated with the proton motive force [Hamsanathan & Musser, 2018]. Given that the central carbon metabolism of *P. putida* is largely based on the Entner-Doudoroff pathway which, compared to the classical glycolysis (Embden-Meyerhof-Parnas) pathway, yields

less ATP and more NAD(P)H per unit of glucose [Chavarría et al, 2013], ATP might be a limiting factor for translocation to the periplasm and usage of a Tat SP could be a better approach in *P. putida*. Formation of inclusion bodies as a result of overcoming the capacity of the Sec system was reported also in *E. coli* expressing heterologous proteins and required modulating the expression levels to equilibrate translation and translocation [Schlegel et al, 2013].

Still, as discussed in the previous section, secretion of heterologous proteins in Gram negative bacteria following translocation to the periplasm is essentially a gamble. No known, usable mechanism for transport of periplasmic proteins through the outer membrane is known, besides engineering a T5SS that is reportedly unable to transport proteins with disulfide bonds (a necessity for PET hydrolases). What is called secretion in most papers then appears to be a leakage of periplasmic proteins that is often not properly investigated by assessing the membrane integrity beyond the lysis/no-lysis dichotomy (see for instance [Ni & Chen, 2009]). Even though high titres of the recombinant protein can be achieved by causing cells to leak periplasmic protein (and even cytoplasmic proteins), this comes at the cost of weakening the cell envelope, potentially increasing the susceptibility of the host to stresses and defeating the purpose of developing novel hosts for use in lower-cost industrial processes, such as would be the case for *P. putida*.

Moreover, if the extracellular production of a recombinant protein is the result of partial disruption of the cell membrane, all the proteins present in the cell compartment that has become exposed to the outside will be released, and the need for the isolation of the target protein from a complex mixture of polypeptides will not be eliminated (see for instance the SDS-PAGE scans from [Shi et al, 2021]).

An alternative could be to bypass the periplasm entirely and induce the secretion of a heterologous protein through a one-step secretion system. In Gram negative bacteria, however, disulfide bonds tend to form in the periplasm so that, for protein that require the formation of disulfide bonds for optimal activity, care would have to be exercised to ensure that the secreted proteins are processed correctly. Secretion of a disulfide bond-containing single-chain Fv antibody fragment was achieved in *E. coli* using the host's native T1SS, with the recombinant protein being observed at high purity and with correct folding in the growth medium [Fernández & De Lorenzo, 2001]. In a more recent example, the flagellar type 3 secretion system of *E. coli* was successfully engineered for secretion of various heterologous proteins, including the cutinase of *Fusarium solani,* although no mention was made of disulfide bonds [Green et al, 2019]. Complete deletion in *P. putida* of chromosomal region coding for the flagellar machinery was even shown to be beneficial to heterologous protein expression and growth rate [Lieder et al, 2015; Martínez-García et al, 2020].

The optimisation of conditions for protein expression was only implemented here at the level of a preliminary screening. At an earlier stage of the project, plans had been drawn for a response surface methodology study on the concentrations of the C-source, N-source, and inducer on the growth rate, and heterologous protein titre and activity. Incubation temperatures during initial growth and after induction were also to be included in the design. Generation of a D-optimal split-plot design, with the incubation temperatures as whole-plot variables and the aforementioned components' concentrations as sub-plot variables, plus a subset of first order interactions ([C-source] x [N-source], T_{growth} x [C-source], $T_{induction}$ x [inducer]), in the models of the responses was chosen as the most appropriate approach to minimize the effort and laboratory footprint required for the design while maximizing the information content of the experiment (see for instance the skpr package for R [Morgan-Wall & Khoury, 2021]; also, [de Aguiar et al, 1995]).

A final note concerns the codon optimisation of the synthetic gene constructs used in this project as multiple papers have reported a decreased expression level when heterologous genes are codon optimised, compared to using the native sequences [Dammeyer et al, 2011; Incha et al, 2020]. Care should be exercised when choosing a codon-optimisation algorithm as, for instance, only focusing on mirroring codon

usage tables might lead to the appearance of new secondary structures in mRNA which in turn lead to lower transcription levels (for a review on the topic, see [Gould et al, 2014]).

Conclusions

In the course of this project, we have successfully assembled a plasmid for the expression of the highly thermostable PET-depolymerase $LCC^{ICCG-KRP}$ in *P. putida*, an emerging workhorse for industrial biotechnology.

Expression levels of the protein of interest have however remained low, but nonetheless the specific activity of the expressed enzyme, estimated from PET-depolymerisation assays, has been shown to be comparable to that of the same enzyme expressed in *E. coli*.

Over the course of four protein expression studies with the transformed strain of *P. putida*, we have observed evidence indicative of cell lysis and formation of inclusion bodies in the cells, although neither could be conclusive proven. Further work would be needed to confirm and elucidate these observations and develop solutions for improved viability of the host and solubility of the heterologous enzyme.

Secretion of the enzyme from the expression host was an additional goal of this project, but no conclusive evidence of secretion of the enzyme fused to a N-terminal Sec pathway-targeting signal peptide could be obtained. The literature on the topic of protein secretion of Gram negative bacteria was consulted and confirmed the general absence of any native mechanism for translocation of periplasmic proteins across the outer membrane. On this topic, attention is brought to potential alternatives for engineering of heterologous protein secretion in Gram negative hosts.

References

1. Abby, S.S., and Rocha, E.P.C. (2012). The Non-Flagellar Type III Secretion System Evolved from the Bacterial Flagellum and Diversified into Host-Cell Adapted Systems. PLOS Genetics 8, e1002983. 10.1371/journal.pgen.1002983.

2. Al-Salem, S.M., Lettieri, P., and Baeyens, J. (2009). Recycling and recovery routes of plastic solid waste (PSW): A review. Waste Management 29, 2625–2643. 10.1016/j.wasman.2009.06.004.

3. Ankenbauer, A., Schäfer, R.A., Viegas, S.C., Pobre, V., Voß, B., Arraiano, C.M., and Takors, R. (2020). Pseudomonas putida KT2440 is naturally endowed to withstand industrial-scale stress conditions. Microb Biotechnol 13, 1145–1161. 10.1111/1751-7915.13571.

4. Aparicio, T., de Lorenzo, V., and Martínez-García, E. (2018). CRISPR/Cas9-Based Counterselection Boosts Recombineering Efficiency in Pseudomonas putida. Biotechnology Journal 13, 1700161. 10.1002/biot.201700161.

5. Aparicio, T., Nyerges, A., Martínez-García, E., and De Lorenzo, V. (2020). High-Efficiency Multi-site Genomic Editing of Pseudomonas putida through Thermoinducible ssDNA Recombineering. iScience 23, 100946. 10.1016/j.isci.2020.100946.

6. Baú, D., Martin, A.J., Mooney, C., Vullo, A., Walsh, I., and Pollastri, G. (2006). Distill: a suite of web servers for the prediction of one-, two- and three-dimensional structural features of proteins. BMC Bioinformatics 7, 402. 10.1186/1471-2105-7-402.

7. Belda, E., van Heck, R.G.A., José Lopez-Sanchez, M., Cruveiller, S., Barbe, V., Fraser, C., Klenk, H.-P., Petersen, J., Morgat, A., Nikel, P.I., et al. (2016). The revisited genome of Pseudomonas putida KT2440 enlightens its value as a robust metabolic chassis. Environ Microbiol 18, 3403–3424. 10.1111/1462-2920.13230.

8. Bell, E.L., Smithson, R., Kilbride, S., Foster, J., Hardy, F.J., Ramachandran, S., Tedstone, A.A., Haigh, S.J., Garforth, A.A., Day, P.J.R., et al. (2022). Directed evolution of an efficient and thermostable PET depolymerase. Nat Catal 5, 673–681. 10.1038/s41929-022-00821-3.

9. Bornhorst, J.A., and Falke, J.J. (2000). Purification of Proteins Using Polyhistidine Affinity Tags. Methods Enzymol 326, 245–254.

10. Brandenberg, O.F., Schubert, O.T., and Kruglyak, L. (2022). Towards synthetic PETtrophy: Engineering Pseudomonas putida for concurrent polyethylene terephthalate (PET) monomer metabolism and PET hydrolase expression. Microb Cell Fact 21, 119. 10.1186/s12934-022-01849-7.

11. Brandon, A.M., Gao, S.-H., Tian, R., Ning, D., Yang, S.-S., Zhou, J., Wu, W.-M., and Criddle, C.S. (2018). Biodegradation of Polyethylene and Plastic Mixtures in Mealworms (Larvae of Tenebrio molitor) and Effects on the Gut Microbiome. Environ. Sci. Technol. 52, 6526–6533. 10.1021/acs.est.8b02301.

12. Buchholz, P.C.F., Feuerriegel, G., Zhang, H., Perez-Garcia, P., Nover, L.-L., Chow, J., Streit, W.R., and Pleiss, J. (2022). Plastics degradation by hydrolytic enzymes: The plastics-active enzymes database—PAZy. Proteins: Structure, Function, and Bioinformatics 90, 1443–1456. 10.1002/prot.26325.

13. Burlage, R.S., Hooper, S.W., and Sayler, G.S. (1989). The TOL (pWW0) catabolic plasmid. Appl Environ Microbiol 55, 1323–1328.

14. Chavarría, M., Nikel, P.I., Pérez-Pantoja, D., and de Lorenzo, V. (2013). The Entner–Doudoroff pathway empowers Pseudomonas putida KT2440 with a high tolerance to oxidative stress. Environmental Microbiology 15, 1772–1785. 10.1111/1462-2920.12069.

15. Choi, K.-H., Kumar, A., and Schweizer, H.P. (2006). A 10-min method for preparation of highly electrocompetent Pseudomonas aeruginosa cells: Application for DNA fragment transfer between chromosomes and plasmid transformation. Journal of Microbiological Methods 64, 391–397. 10.1016/j.mimet.2005.06.001.

16. Chow, J., Perez-Garcia, P., Dierkes, R., and Streit, W.R. (2023). Microbial enzymes will offer limited solutions to the global plastic pollution crisis. Microbial Biotechnology 16, 195–217. 10.1111/1751-7915.14135.

17. Cook, T.B., Rand, J.M., Nurani, W., Courtney, D.K., Liu, S.A., and Pfleger, B.F. (2018). Genetic tools for reliable gene expression and recombineering in Pseudomonas putida. Journal of Industrial Microbiology and Biotechnology 45, 517–527. 10.1007/s10295-017-2001-5.

18. Cook, T.B., Jacobson, T.B., Venkataraman, M.V., Hofstetter, H., Amador-Noguez, D., Thomas, M.G., and Pfleger, B.F. (2021). Stepwise genetic engineering of Pseudomonas putida enables robust heterologous production of prodigiosin and glidobactin A. Metabolic Engineering 67, 112–124. 10.1016/j.ymben.2021.06.004.

19. Cui, L., Qiu, Y., Liang, Y., Du, C., Dong, W., Cheng, C., and He, B. (2021). Excretory expression of IsPETase in E. coli by an enhancer of signal peptides and enhanced PET hydrolysis. International Journal of Biological Macromolecules 188, 568–575. 10.1016/j.ijbiomac.2021.08.012.

20. Cui, Y., Chen, Y., Liu, X., Dong, S., Tian, Y., Qiao, Y., Mitra, R., Han, J., Li, C., Han, X., et al. (2021). Computational Redesign of a PETase for Plastic Biodegradation under Ambient Condition by the GRAPE Strategy. ACS Catal. 11, 1340–1350. 10.1021/acscatal.0c05126.

21. Dammeyer, T., Steinwand, M., Krüger, S.-C., Dübel, S., Hust, M., and Timmis, K.N. (2011). Efficient production of soluble recombinant single chain Fv fragments by a Pseudomonas putida strain KT2440 cell factory. Microbial Cell Factories 10, 11. 10.1186/1475-2859-10-11.

22. Danilevich, V.N., Petrovskaya, L.E., and Grishin, E.V. (2006). Rapid and efficient extraction of soluble proteins from Gram-negative microorganisms without disruption of cell walls. Russ J Bioorg Chem 32, 521–528. 10.1134/S1068162006060045.

23. de Aguiar, P.F., Bourguignon, B., Khots, M.S., Massart, D.L., and Phan-Than-Luu, R. (1995). D-optimal designs. Chemometrics and Intelligent Laboratory Systems 30, 199–210. 10.1016/0169-7439(94)00076-X.

24. De Vrind, J.P.M., Brouwers, G.J., Corstjens, P.L.A.M., den Dulk, J., and de Vrind-de Jong, E.W. (1998). The Cytochrome c Maturation Operon Is Involved in Manganese Oxidation in Pseudomonas putida GB-1. Appl Environ Microbiol 64, 3556–3562.

25. De Vrind, J., De Groot, A., Brouwers, G.J., Tommassen, J., and De Vrind-de Jong, E. (2003). Identification of a novel Gsp-related pathway required for secretion of the manganese-oxidizing factor of Pseudomonas putida strain GB-1. Molecular Microbiology 47, 993–1006. 10.1046/j.1365-2958.2003.03339.x.

26. Eberl, A., Heumann, S., Brückner, T., Araujo, R., Cavaco-Paulo, A., Kaufmann, F., Kroutil, W., and Guebitz, G.M. (2009). Enzymatic surface hydrolysis of poly(ethylene terephthalate) and bis(benzoyloxyethyl) terephthalate by lipase and cutinase in the presence of surface active molecules. Journal of Biotechnology 143, 207–212. 10.1016/j.jbiotec.2009.07.008.

27. Erkut, E. (2021). Bacterial signal peptides: structure, optimization, and applications. Eureka 6. 10.29173/eureka28759.

28. Fecker, T., Galaz-Davison, P., Engelberger, F., Narui, Y., Sotomayor, M., Parra, L.P., and Ramírez-Sarmiento, C.A. (2018). Active Site Flexibility as a Hallmark for Efficient PET Degradation by I. sakaiensis PETase. Biophysical Journal 114, 1302–1312. 10.1016/j.bpj.2018.02.005.

29. Fernández, L.A., and De Lorenzo, V. (2001). Formation of disulphide bonds during secretion of proteins through the periplasmic-independent type I pathway. Molecular Microbiology 40, 332–346. 10.1046/j.1365-2958.2001.02410.x.

30. Ferreira, R. da G., Azzoni, A.R., and Freitas, S. (2018). Techno-economic analysis of the industrial production of a low-cost enzyme using E. coli: the case of recombinant β-glucosidase. Biotechnol Biofuels 11, 81. 10.1186/s13068-018-1077-0.

31. Filloux, A. (2004). The underlying mechanisms of type II protein secretion. Biochimica et Biophysica Acta (BBA) - Molecular Cell Research 1694, 163–179. 10.1016/j.bbamcr.2004.05.003.

32. Filloux, A. (2022). Bacterial protein secretion systems: Game of types: This article is part of the Bacterial Cell Envelopes collection. Microbiology 168. 10.1099/mic.0.001193.

33. Freudl, R. (2018). Signal peptides for recombinant protein secretion in bacterial expression systems. Microb Cell Fact 17, 52. 10.1186/s12934-018-0901-3.

34. Fujita, M., Torigoe, K., Nakada, T., Tsusaki, K., Kubota, M., Sakai, S., and Tsujisaka, Y. (1989). Cloning and nucleotide sequence of the gene (amyP) for maltotetraose-forming amylase from Pseudomonas stutzeri MO-19. J Bacteriol 171, 1333–1339. 10.1128/jb.171.3.1333-1339.1989.

35. Garcia, J.M., and Robertson, M.L. (2017). The future of plastics recycling. Science 358, 870–872. 10.1126/science.aaq0324.

36. Gawin, A., Valla, S., and Brautaset, T. (2017). The XylS/Pm regulator/promoter system and its use in fundamental studies of bacterial gene expression, recombinant protein production and metabolic engineering. Microbial Biotechnology 10, 702–718. 10.1111/1751-7915.12701.

37. Georgiou, G., and Valax, P. (1999). Isolating inclusion bodies from bacteria. In Methods in Enzymology (Elsevier), pp. 48–58. 10.1016/S0076-6879(99)09005-9.

38. Geyer, R. (2020). Production, use, and fate of synthetic polymers. In Plastic Waste and Recycling (Elsevier), pp. 13–32. 10.1016/B978-0-12-817880-5.00002-5.

39. Geyer, R., Jambeck, J.R., and Law, K.L. (2017). Production, use, and fate of all plastics ever made. Sci Adv 3, e1700782. 10.1126/sciadv.1700782.

40. Gould, N., Hendy, O., and Papamichail, D. (2014). Computational Tools and Algorithms for Designing Customized Synthetic Genes. Front. Bioeng. Biotechnol. 2. 10.3389/fbioe.2014.00041.

41. Grömping, U. (2014). R Package FrF2 for Creating and Analyzing Fractional Factorial 2-Level Designs. Journal of Statistical Software 56, 1–56. 10.18637/jss.v056.i01.

42. Gruber, A.R., Lorenz, R., Bernhart, S.H., Neubock, R., and Hofacker, I.L. (2008). The Vienna RNA Websuite. Nucleic Acids Research 36, W70–W74. 10.1093/nar/gkn188.

43. Hamsanathan, S., and Musser, S.M. (2018). The Tat protein transport system: intriguing questions and conundrums. FEMS Microbiol Lett 365, fny123. 10.1093/femsle/fny123.

44. Hedstrom, L. (2010). Enzyme Specificity and Selectivity. In Encyclopedia of Life Sciences (Wiley). 10.1002/9780470015902.a0000716.pub2.

45. Herrero Acero, E., Ribitsch, D., Steinkellner, G., Gruber, K., Greimel, K., Eiteljoerg, I., Trotscha, E., Wei, R., Zimmermann, W., Zinn, M., et al. (2011). Enzymatic Surface Hydrolysis of PET: Effect of Structural Diversity on Kinetic Properties of Cutinases from Thermobifida. Macromolecules 44, 4632–4640. 10.1021/ma200949p.

46. Huang, J., Veksha, A., Chan, W.P., Giannis, A., and Lisak, G. (2022). Chemical recycling of plastic waste for sustainable material management: A prospective review on catalysts and processes. Renewable and Sustainable Energy Reviews 154, 111866. 10.1016/j.rser.2021.111866.

47. Incha, M.R., Thompson, M.G., Blake-Hedges, J.M., Liu, Y., Pearson, A.N., Schmidt, M., Gin, J.W., Petzold, C.J., Deutschbauer, A.M., and Keasling, J.D. (2020). Leveraging host metabolism for bisdemethoxycurcumin production in Pseudomonas putida. Metabolic Engineering Communications 10, e00119. 10.1016/j.mec.2019.e00119.

48. Jevševar, S., Gaberc-Porekar, V., Fonda, I., Podobnik, B., Grdadolnik, J., and Menart, V. (2005). Production of Nonclassical Inclusion Bodies from Which Correctly Folded Protein Can Be Extracted. Biotechnology Progress 21, 632–639. 10.1021/bp0497839.

49. Joo, S., Cho, I.J., Seo, H., Son, H.F., Sagong, H.-Y., Shin, T.J., Choi, S.Y., Lee, S.Y., and Kim, K.-J. (2018). Structural insight into molecular mechanism of poly(ethylene terephthalate) degradation. Nat Commun 9, 382. 10.1038/s41467-018-02881-1.

50. Köbbing, S. (2020). Development of synthetic biology tools for Pseudomonas putida 1. Auflage. (Apprimus Verlag).

51. Korbie, D.J., and Mattick, J.S. (2008). Touchdown PCR for increased specificity and sensitivity in PCR amplification. Nat Protoc 3, 1452–1456. 10.1038/nprot.2008.133.

52. Korotkov, K.V., and Sandkvist, M. (2019). Architecture, Function, and Substrates of the Type II Secretion System. EcoSal Plus 8, ecosalplus.ESP-0034-2018. 10.1128/ecosalplus.ESP-0034-2018.

53. Korotkov, K.V., Sandkvist, M., and Hol, W.G.J. (2012). The type II secretion system: biogenesis, molecular architecture and mechanism. Nat Rev Microbiol 10, 336–351. 10.1038/nrmicro2762.

54. Leslie, H.A., Leonards, P.E.G., Brandsma, S.H., de Boer, J., and Jonkers, N. (2016). Propelling plastics into the circular economy — weeding out the toxics first. Environment International 94, 230–234. 10.1016/j.envint.2016.05.012.

55. Leyton, D.L., Sevastsyanovich, Y.R., Browning, D.F., Rossiter, A.E., Wells, T.J., Fitzpatrick, R.E., Overduin, M., Cunningham, A.F., and Henderson, I.R. (2011). Size and conformation limits to secretion of disulfide-bonded loops in autotransporter proteins. J Biol Chem 286, 42283–42291. 10.1074/jbc.M111.306118.

56. Lieder, S., Nikel, P.I., De Lorenzo, V., and Takors, R. (2015). Genome reduction boosts heterologous gene expression in Pseudomonas putida. Microb Cell Fact 14, 23. 10.1186/s12934-015-0207-7.

57. Lu, H., Diaz, D.J., Czarnecki, N.J., Zhu, C., Kim, W., Shroff, R., Acosta, D.J., Alexander, B.R., Cole, H.O., Zhang, Y., et al. (2022). Machine learning-aided engineering of hydrolases for PET depolymerization. Nature 604, 662–667. 10.1038/s41586-022-04599-z.

58. Manoil, C., and Beckwith, J. (1985). TnphoA: a transposon probe for protein export signals. Proc. Natl. Acad. Sci. U.S.A. 82, 8129–8133. 10.1073/pnas.82.23.8129.

59. Martínez-García, E., Calles, B., Arévalo-Rodríguez, M., and de Lorenzo, V. (2011). pBAM1: an all-synthetic genetic tool for analysis and construction of complex bacterial phenotypes. BMC Microbiology 11, 38. 10.1186/1471-2180-11-38.

60. Martínez-García, E., Fraile, S., Algar, E., Aparicio, T., Velázquez, E., Calles, B., Tas, H., Blázquez, B., Martín, B., Prieto, C., et al. (2023). SEVA 4.0: an update of the Standard European Vector Architecture database for advanced analysis and programming of bacterial phenotypes. Nucleic Acids Research 51, D1558–D1567. 10.1093/nar/gkac1059.

61. Martínez-García, E., Fraile, S., Espeso, D.R., Vecchietti, D., Bertoni, G., and Lorenzo, V. de (2020). The naked cell: emerging properties of a surfome-streamlined Pseudomonas putida strain. Preprint at bioRxiv, 10.1101/2020.05.17.100628 10.1101/2020.05.17.100628.

62. Martins dos Santos, V.A.P., Timmis, K.N., Tümmler, B., and Weinel, C. (2004). Genomic Features of Pseudomonas putida Strain KT2440. In Pseudomonas: Volume 1 Genomics, Life Style and Molecular Architecture, J.-L. Ramos, ed. (Springer US), pp. 77–112. 10.1007/978-1-4419-9086-0_3.

63. McGlade, J., Fahim, I.S., Green, D., and Landrigan, P. (2021). From Pollution to Solution: A global assessment of marine litter and plastic pollution (UNEP (United Nations Environmental Programme)).

64. Millar, R., Rahmanpour, R., Yuan, E.W.J., White, C., and Bugg, T.D.H. (2017). Esterase EstK from Pseudomonas putida mt-2: An enantioselective acetylesterase with activity for deacetylation of xylan and poly(vinylacetate). Biotechnology and Applied Biochemistry 64, 803–809. 10.1002/bab.1536.

65. Mirabello, C., and Pollastri, G. (2013). Porter, PaleAle 4.0: high-accuracy prediction of protein secondary structure and relative solvent accessibility. Bioinformatics 29, 2056–2058. 10.1093/bioinformatics/btt344.

66. Mirzadeh, K., Shilling, P.J., Elfageih, R., Cumming, A.J., Cui, H.L., Rennig, M., Nørholm, M.H.H., and Daley, D.O. (2020). Increased production of periplasmic proteins in Escherichia coli by directed evolution of the translation initiation region. Microbial Cell Factories 19, 85. 10.1186/s12934-020-01339-8.

67. Morgan-Wall, T., and Khoury, G. (2021). Optimal Design Generation and Power Evaluation in R : The skpr Package. J. Stat. Soft. 99. 10.18637/jss.v099.i01.

68. Ni, Y., and Chen, R. (2009). Extracellular recombinant protein production from Escherichia coli. Biotechnol Lett 31, 1661–1670. 10.1007/s10529-009-0077-3.

69. Nikel, P.I., Chavarría, M., Fuhrer, T., Sauer, U., and de Lorenzo, V. (2015). Pseudomonas putida KT2440 Strain Metabolizes Glucose through a Cycle Formed by Enzymes of the Entner-Doudoroff, Embden-Meyerhof-Parnas, and Pentose Phosphate Pathways*. Journal of Biological Chemistry 290, 25920–25932. 10.1074/jbc.M115.687749.

70. Okan, M., Aydin, H.M., and Barsbay, M. (2019). Current approaches to waste polymer utilization and minimization: a review. J of Chemical Tech & Biotech 94, 8–21. 10.1002/jctb.5778.

71. Payne, S.H., Bonissone, S., Wu, S., Brown, R.N., Ivankov, D.N., Frishman, D., Paša-Tolić, L., Smith, R.D., and Pevzner, P.A. (2012). Unexpected Diversity of Signal Peptides in Prokaryotes. mBio 3, 10.1128/mbio.00339-12. 10.1128/mbio.00339-12.

72. Perez-Garcia, P., Chow, J., Costanzi, E., Gurschke, M., Dittrich, J., Dierkes, R.F., Molitor, R., Applegate, V., Feuerriegel, G., Tete, P., et al. (2023). An archaeal lid-containing feruloyl esterase degrades polyethylene terephthalate. Commun Chem 6, 1–13. 10.1038/s42004-023-00998-z.

73. Putker, F., Tommassen-van Boxtel, R., Stork, M., Rodríguez-Herva, J.J., Koster, M., and Tommassen, J. (2013). The type II secretion system (X cp) of P seudomonas putida is active and involved in the secretion of phosphatases. Environmental Microbiology 15, 2658–2671. 10.1111/1462-2920.12115.

74. Ragaert, K., Delva, L., and Van Geem, K. (2017). Mechanical and chemical recycling of solid plastic waste. Waste Management 69, 24–58. 10.1016/j.wasman.2017.07.044.

75. Réjasse, A., Waeytens, J., Deniset-Besseau, A., Crapart, N., Nielsen-Leroux, C., and Sandt, C. (2022). Plastic biodegradation: Do Galleria mellonella Larvae Bioassimilate Polyethylene? A Spectral Histology Approach Using Isotopic Labeling and Infrared Microspectroscopy. Environ. Sci. Technol. 56, 525–534. 10.1021/acs.est.1c03417.

76. Rothman, S.C., and Kirsch, J.F. (2003). How Does an Enzyme Evolved In vitro Compare to Naturally Occurring Homologs Possessing the Targeted Function? Tyrosine Aminotransferase from Aspartate Aminotransferase. Journal of Molecular Biology 327, 593–608. 10.1016/S0022-2836(03)00095-0.

77. Roux, M., and Varrone, C. (2021). Assessing the Economic Viability of the Plastic Biorefinery Concept and Its Contribution to a More Circular Plastic Sector. Polymers 13, 3883. 10.3390/polym13223883.

78. Ryan, B.J., and Kinsella, G.K. (2017). Differential Precipitation and Solubilization of Proteins. In Protein Chromatography Methods in Molecular Biology., D. Walls and S. T. Loughran, eds. (Springer New York), pp. 191–208. 10.1007/978-1-4939-6412-3_10.

79. Sanluis-Verdes, A., Colomer-Vidal, P., Rodriguez-Ventura, F., Bello-Villarino, M., Spinola-Amilibia, M., Ruiz-Lopez, E., Illanes-Vicioso, R., Castroviejo, P., Aiese Cigliano, R., Montoya, M., et al. (2022). Wax worm saliva and the enzymes therein are the key to polyethylene degradation by Galleria mellonella. Nat Commun 13, 5568. 10.1038/s41467-022-33127-w.

80. Shi, L., Liu, P., Tan, Z., Zhao, W., Gao, J., Gu, Q., Ma, H., Liu, H., and Zhu, L. (2023). Complete Depolymerization of PET Wastes by an Evolved PET Hydrolase from Directed Evolution. Angew Chem Int Ed 62, e202218390. 10.1002/anie.202218390.

81. Silva-Rocha, R., Martínez-García, E., Calles, B., Chavarría, M., Arce-Rodríguez, A., De Las Heras, A., Páez-Espino, A.D., Durante-Rodríguez, G., Kim, J., Nikel, P.I., et al. (2013). The Standard European Vector Architecture (SEVA): a coherent platform for the analysis and deployment of complex prokaryotic phenotypes. Nucleic Acids Research 41, D666–D675. 10.1093/nar/gks1119.

82. Singh, A., Upadhyay, V., Upadhyay, A.K., Singh, S.M., and Panda, A.K. (2015). Protein recovery from inclusion bodies of Escherichia coli using mild solubilization process. Microbial Cell Factories 14, 41. 10.1186/s12934-015-0222-8.

83. Studier, W.F., Rosenberg, A.H., Dunn, J.J., and Dubendorff, J.W. (1990). Use of T7 RNA polymerase to direct expression of cloned genes. Methods in Enzymology 185, 60–89. https://doi.org/10.1016/0076-6879(90)85008-C.

84. Su, L., Woodard, R.W., Chen, J., and Wu, J. (2013). Extracellular Location of Thermobifida fusca Cutinase Expressed in Escherichia coli BL21(DE3) without Mediation of a Signal Peptide. Applied and Environmental Microbiology 79, 4192–4198. 10.1128/AEM.00239-13.

85. Sulaiman, S., Yamato, S., Kanaya, E., Kim, J.-J., Koga, Y., Takano, K., and Kanaya, S. (2012). Isolation of a Novel Cutinase Homolog with Polyethylene Terephthalate-Degrading Activity from Leaf-Branch Compost by Using a Metagenomic Approach. Appl Environ Microbiol 78, 1556–1562. 10.1128/AEM.06725-11.

86. Suominen, I., Karp, M., Lautamo, J., Knowles, J., and Mantsälä, P. (1987). Thermostable Alpha Amylase of Bacillus Stearothermophilus: Cloning, Expression, and Secretion by Escherichia Coli. In Extracellular Enzymes of Microorganisms, J. Chaloupka and V. Krumphanzl, eds. (Springer US), pp. 129–137. 10.1007/978-1-4684-1274-1_16.

87. Taylor, G., Hoare, M., Gray, D.R., and Marston, F.A.O. (1986). Size and Density of Protein Inclusion Bodies. Nat Biotechnol 4, 553–557. 10.1038/nbt0686-553.

88. Teufel, F., Almagro Armenteros, J.J., Johansen, A.R., Gíslason, M.H., Pihl, S.I., Tsirigos, K.D., Winther, O., Brunak, S., Von Heijne, G., and Nielsen, H. (2022). SignalP 6.0 predicts all five types of signal peptides using protein language models. Nat Biotechnol 40, 1023–1025. 10.1038/s41587-021-01156-3.

89. Tournier, V., Topham, C.M., Gilles, A., David, B., Folgoas, C., Moya-Leclair, E., Kamionka, E., Desrousseaux, M.-L., Texier, H., Gavalda, S., et al. (2020). An engineered PET depolymerase to break down and recycle plastic bottles. Nature 580, 216–219. 10.1038/s41586-020-2149-4.

90. Volke, D.C., Turlin, J., Mol, V., and Nikel, P.I. (2020). Physical decoupling of XylS/Pm regulatory elements and conditional proteolysis enable precise control of gene expression in Pseudomonas putida. Microbial Biotechnology 13, 222–232. 10.1111/1751-7915.13383.

91. Wirth, N.T., Kozaeva, E., and Nikel, P.I. (2020). Accelerated genome engineering of Pseudomonas putida by I-SceI—mediated recombination and CRISPR-Cas9 counterselection. Microbial Biotechnology 13, 233–249. 10.1111/1751-7915.13396.

92. Wirth, N.T., Kozaeva, E., and Nikel, P.I. (2020). Accelerated genome engineering of Pseudomonas putida by I- Sce I—mediated recombination and CRISPR -Cas9 counterselection. Microbial Biotechnology 13, 233–249. 10.1111/1751-7915.13396.

93. World Bank (2022). Where Is the Value in the Chain?: Pathways out of Plastic Pollution (The World Bank) 10.1596/978-1-4648-1881-3.

94. Yang, S.-S., Wu, W.-M., Brandon, A.M., Fan, H.-Q., Receveur, J.P., Li, Y., Wang, Z.-Y., Fan, R., McClellan, R.L., Gao, S.-H., et al. (2018). Ubiquity of polystyrene digestion and biodegradation within yellow mealworms, larvae of Tenebrio molitor Linnaeus (Coleoptera: Tenebrionidae). Chemosphere 212, 262–271. 10.1016/j.chemosphere.2018.08.078.

95. Yang, Y., Yang, J., Wu, W.-M., Zhao, J., Song, Y., Gao, L., Yang, R., and Jiang, L. (2015). Biodegradation and Mineralization of Polystyrene by Plastic-Eating Mealworms: Part 1. Chemical and Physical Characterization and Isotopic Tests. Environ. Sci. Technol. 49, 12080–12086. 10.1021/acs.est.5b02661.

96. Yang, Y., Yang, J., Wu, W.-M., Zhao, J., Song, Y., Gao, L., Yang, R., and Jiang, L. (2015). Biodegradation and Mineralization of Polystyrene by Plastic-Eating Mealworms: Part 2. Role of Gut Microorganisms. Environ. Sci. Technol. 49, 12087–12093. 10.1021/acs.est.5b02663.

97. Yoshida, S., Hiraga, K., Takehana, T., Taniguchi, I., Yamaji, H., Maeda, Y., Toyohara, K., Miyamoto, K., Kimura, Y., and Oda, K. (2016). A bacterium that degrades and assimilates poly(ethylene terephthalate). Science 351, 1196–1199. 10.1126/science.aad6359.

98. Zhang, F., Zhao, Y., Wang, D., Yan, M., Zhang, J., Zhang, P., Ding, T., Chen, L., and Chen, C. (2021). Current technologies for plastic waste treatment: A review. Journal of Cleaner Production 282, 124523. 10.1016/j.jclepro.2020.124523.

99. Zhang, W., Lu, J., Zhang, S., Liu, L., Pang, X., and Lv, J. (2018). Development an effective system to expression recombinant protein in E. coli via comparison and optimization of signal peptides: Expression of Pseudomonas fluorescens BJ-10 thermostable lipase as case study. Microbial cell factories *17*, 50. 10.1186/s12934-018-0894-y.

100. Plastics – the Facts 2022 (2022). (PlasticsEurope AISBL).

Appendix

A. Protein-coding sequences submitted, codon-optimised for *P. putida*

> $LCC^{ICCG-KRP}$ (as submitted to Gene Universal; small letters correspond to signal peptide)

atgagccacatcctgcgagccgccgtattggcggcgatgctgttgccgttgccgtccatggccAGCAACCCGTACCAGCGTGGACCTAACCCG
ACCCGCTCGGCTCTGACCGCCGACGGTCCATTCAGCGTCAAGACCTATACAGTCAGTCGCTTGAGCGTAAGTGGCTTC
GGGGGCGGCCGCATCTACTACCCGACGGGCACCTCGCTGACTTTCGGCGGTATCGCTATGTCGCCCGGGTACACCGC
GGATGCGAGCAGCTTGGCCTGGCTGGGCCGTCGACTCGCATCGCATGGCTTCGTCGTCCTGGTTATCAACACCAACTC
ACGCTTCGATGGCCCAGACAGCCGGGCCAGCCAGCTCTCCGCCGCGCTGAACTATCTGCGTACCTCGAGCCCGTCCGC
CGTACGCGCCAGGCTAGACGCAAATCGCTTGGCCGTGGCCGGCCACAGTATGGGCGGGGGCGGTACTCTGCGGATC
GCCGAGCAAAATCCGAGCCTTAAGGCCGCCGTGCCACTGACCCCGTGGCACACGGATAAGACCTTTAACACCTCGGTC
CCGGTGCTCATCGTGGGTGCAGAAGCGGACACGGTGGCCCCGGTGTCCCAGCACGCGATTCCCTTTTATCAAAACCTG
CCTTCCACCACACCCAAGGTGTACGTGGAGCTGTGCAATGCTTCTCATATTGCCCCCAACTCGCCGAATGCCGCGATCA
GCGTGTACACCATCAGCTGGATGAAACTGTGGGTCGACAACGACACGCGCTACCGCCAGTTCCTGTGCAACGTTAAC
GACCCGGCGCTGTGCGACTTCCGCACCAACAACCGGCACTGTCAGCTCGAGCACCACCACCACCACCACTAA

> $LCC^{ICCG-KRP}$ (as received from Gene Universal, small letters correspond to signal peptide)
atgagccacatcctgcgcgccgccgtgctggccgccatgctgctgccgctgccgagcatggccAGCAACCCGTACCAGCGCGGCCCGAACCC
GACCCGTAGCGCCCTGACCGCCGACGGCCCGTTCAGCGTGAAGACCTACACCGTGAGCCGCCTGAGCGTGAGCGGCT
TCGGCGGCGGCCGTATCTACTACCCGACCGGCACCAGCCTGACCTTCGGCGGCATCGCCATGAGCCCGGGCTACACC
GCCGACGCCAGCAGCCTGGCCTGGCTGGGCCGTCGTCTGGCCAGCCATGGCTTCGTGGTGCTGGTCATTAACACCAA
CAGCCGCTTCGACGGCCCGGACAGCCGCGCCAGCCAGCTGAGCGCCGCCCTGAACTACCTGCGCACCAGCAGCCCGA
GCGCCGTGCGTGCCCGTCTGGATGCCAACCGCCTGGCCGTGGCCGGCCATAGCATGGGCGGCGGCGGCACCCTGCGT
ATCGCCGAGCAGAACCCGAGCCTGAAGGCCGCCGTGCCGCTGACCCCGTGGCATACCGACAAGACCTTCAACACCAG
CGTGCCGGTGCTGATCGTGGGCGCCGAAGCCGACACCGTGGCCCCGGTGAGCCAGCATGCCATCCCGTTCTACCAGA
ACCTGCCGAGCACCACCCCGAAGGTGTACGTGGAACTGTGCAACGCCAGCCACATCGCCCCGAACAGCCCGAACGCC
GCCATCAGCGTGTACACCATCAGCTGGATGAAGCTGTGGGTGGACAACGACACCCGCTACCGCCAGTTCCTGTGCAA
CGTGAACGACCCGGCCCTGTGCGACTTCCGCACCAACAACCGCCACTGCCAGCTGGAACACCACCACCACCATCACTG
A

> FAST-IcPETase (as submitted to Gene Universal; small letters correspond to signal peptide)

atgagccacatcctgcgagccgccgtattggcggcgatgctgttgccgttgccgtccatggccCAGACCAACCCATACGCGCGCGGGCCGAA
TCCGACGGCCGCGTCACTGGAAGCCAGCGCGGGCCCGTTCACAGTTCGGAGCTTCACCGTCAGCCGCCCAAGCGGTT
ACGGAGCCGGCACTGTGTACTATCCGACCAATGCCGGGGGCACCGTGGGCGCAATTGCGATTGTCCCCGGCTATACC
GCGCGCCAGTCTAGCATCAAATGGTGGGGCCCGCGCCTTGCGTCGCACGGCTTCGTGGTGATCACCATCGACACGAA
CTCCACTCTGGACCAGCCGGAGTCGCGTTCAAGCCAACAGATGGCTGCGCTGCGTCAGGTGGCCAGCCTCAATGGCA
CCAGTTCGAGCCCCATCTACGGGAAGGTTGACACCGCACGGATGGGCGTGATGGGCTGGTCCATGGGCGGCGGTGG
CAGCCTGATCTCCGCTGCGAACAACCCCTCGCTGAAGGCCGCTGCCCCTCAGGCCCCCTGGCATTCCAGCACCAACTTC
AGCAGCGTCACGGTACCTACCCTGATCTTCGCCTGCGAGAACGACTCGATCGCCCCGGTCAACTCGTCCGCCTTGCCG
ATCTACGACAGTATGAGCCAGAACGCCAAGCAATTCCTGGAAATCAAGGGCGGTTCCCACTCGTGCGCCAATAGCGG
TAACTCGAACCAGGCCCTGATAGGCAAAAAGGGTGTGGCCTGGATGAAGCGCTTTATGGATAACGATACCCGCTACA
GCACCTTTGCATGCGAGAACCCAAACTCTACCGCAGTGTCGGACTTCCGAACAGCCAACTGTAGTTTGGAACTCGAGC
ACCACCACCACCACCACTAA

> FAST-IcPETase (as received from Gene Universal, small letters correspond to signal peptide)

atgagccacatcctgcgcgccgccgtgctggccgccatgctgctgccgctgccgagcatggccCAGACCAACCCGTACGCCCGCGGCCCGAAC
CCGACCGCCGCCAGCCTGGAGGCCAGCGCCGGCCCGTTCACCGTGCGTAGCTTCACCGTGAGCCGCCCGAGCGGCTAC
GGCGCCGGCACCGTGTATTACCCGACCAACGCCGGCGGCACCGTGGGCGCCATCGCCATCGTGCCGGGCTACACCGCC
CGCCAGAGCAGCATCAAGTGGTGGGGCCCGCGCCTGGCCAGCCATGGCTTCGTGGTCATTACCATCGACACCAACAGC

ACCCTGGACCAGCCGGAAAGCCGCAGCAGCCAGCAGATGGCCGCCCTGCGTCAGGTGGCCAGCCTGAACGGCACCAG
CAGCAGCCCGATCTACGGCAAGGTGGACACCGCCCGCATGGGCGTGATGGGCTGGAGCATGGGCGGCGGCGGCAGCC
TGATCAGCGCCGCCAACAACCCGAGCCTGAAGGCCGCCGCCCCGCAGGCCCCGTGGCACAGCAGCACCAACTTCAGCA
GCGTGACCGTGCCGACCCTGATCTTCGCCTGCGAAAACGACAGCATCGCCCCGGTGAACAGCAGCGCCCTGCCGATCTA
CGACAGCATGAGCCAGAACGCCAAGCAGTTCCTGGAGATCAAGGGCGGCAGCCACAGCTGCGCCAACAGCGGCAACA
GCAACCAGGCCCTGATCGGCAAGAAGGGCGTGGCCTGGATGAAGCGCTTCATGGACAACGACACCCGCTACAGCACCT
TCGCCTGCGAGAACCCGAACAGCACCGCCGTGAGCGACTTCCGCACCGCCAACTGCAGCCTGGAACTGGAGCACCACC
ACCACCATCACTGA

B. Maps of plasmids received by Gene Universal and assembled expression vectors

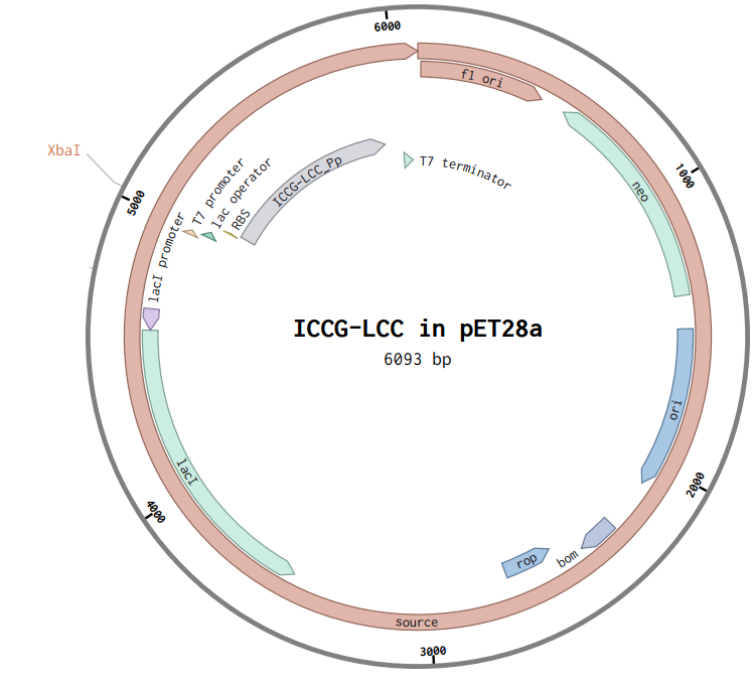

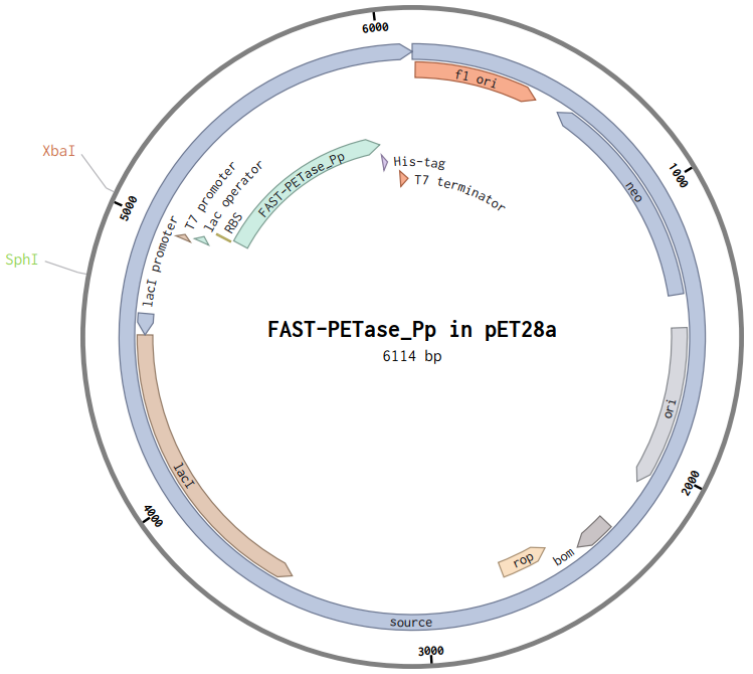

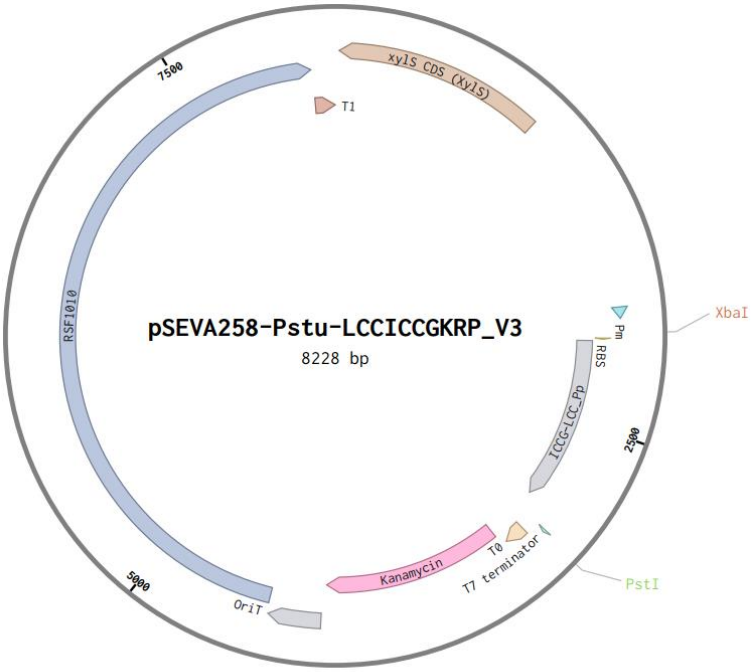
pSEVA258-Pstu-LCCICCGKRP_V3
8228 bp
7500
xylS CDS (XylS)
T1
RSF1010
Pm
RBS
ICCG-LCC_Pp
2500
XbaI
Kanamycin
T0
T7 terminator
PstI
5000
OriT

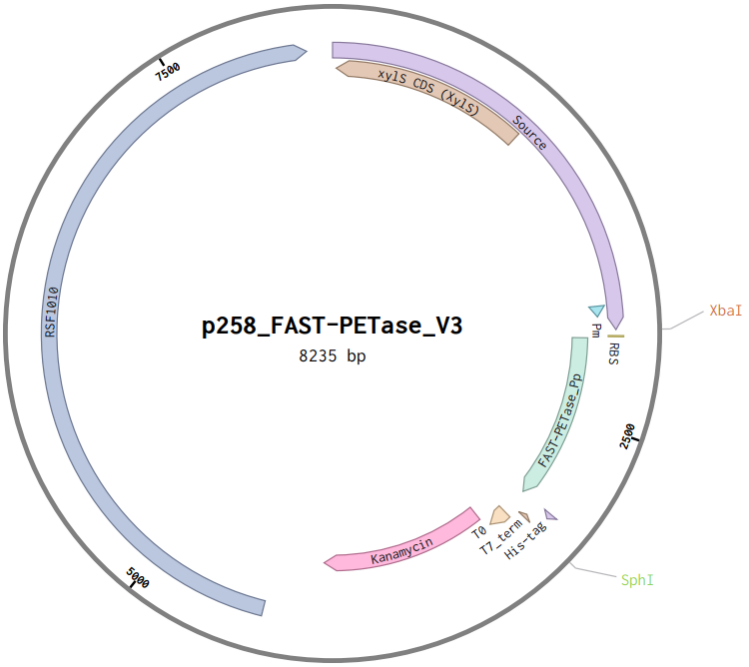
p258_FAST-PETase_V3
8235 bp
7500
xylS CDS (XylS)
Source
RSF1010
Pm
RBS
FAST-PETase_Pp
2500
XbaI
Kanamycin
T0
T7_term
His-tag
SphI
5000